Apoptosis (2019) 24:221–244
https://doi.org/10.1007/s10495-019-01523-1

REVIEW

Targeting phosphatidylserine for radionuclide-based molecular imaging of apoptosis

Melinda Wuest[1] · Amanda Perreault[1] · Susan Richter[1] · James C. Knight[2] · Frank Wuest[1]

Published online: 25 January 2019

Abstract

One major characteristic of programmed cell death (apoptosis) results in the increased expression of phosphatidylserine (PS) on the outer membrane of dying cells. Consequently, PS represents an excellent target for non-invasive imaging of apoptosis by single-photon emission computed tomography (SPECT) and positron emission tomography (PET). Annexin V is a 36 kDa protein which binds with high affinity to PS in the presence of Ca^{2+} ions. This makes radiolabeled annexins valuable apoptosis imaging agents for clinical and biomedical research applications for monitoring apoptosis in vivo. However, the use of radiolabeled annexin V for in vivo imaging of cell death has been met with a variety of challenges which have prevented its translation into the clinic. These difficulties include: complicated and time-consuming radiolabeling procedures, sub-optimal biodistribution, inadequate pharmacokinetics leading to poor tumour-to-blood contrast ratios, reliance upon Ca^{2+} concentrations in vivo, low tumor tissue penetration, and an incomplete understanding of what constitutes the best imaging protocol following induction of apoptosis. Therefore, new concepts and improved strategies for the development of PS-binding radiotracers are needed. Radiolabeled PS-binding peptides and various Zn(II) complexes as phosphate chemosensors offer an innovative strategy for radionuclide-based molecular imaging of apoptosis with PET and SPECT. Radiolabeled peptides and Zn(II) complexes provide several advantages over annexin V including better pharmacokinetics due to their smaller size, better availability, simpler synthesis and radiolabeling strategies as well as facilitated tissue penetration due to their smaller size and faster blood clearance profile allowing for optimized image contrast. In addition, peptides can be structurally modified to improve metabolic stability along with other pharmacokinetic and pharmacodynamic properties. The present review will summarize the current status of radiolabeled annexins, peptides and Zn(II) complexes developed as radiotracers for imaging apoptosis through targeting PS utilizing PET and SPECT imaging.

Keywords Phosphatidylserine · Positron emission tomography (PET) · Single photon emission computed tomography (SPECT) · Annexin V · Peptides · Molecular imaging

✉ Frank Wuest
wuest@ualberta.ca

Melinda Wuest
mwuest@ualberta.ca

Amanda Perreault
aperreau@ualberta.ca

Susan Richter
srichter@ualberta.ca

James C. Knight
james.knight2@ncl.ac.uk

[1] Department of Oncology, Cross Cancer Institute, University of Alberta, 11560 University Avenue, Edmonton, AB T6G 1Z2, Canada

[2] School of Natural and Environmental Sciences, Newcastle University, Newcastle upon Tyne NE1 7RU, UK

Introduction

Apoptosis is a natural, tightly controlled process of programmed cell death that has an important role in normal physiological processes such as embryonic development, immune system regulation, and tissue homeostasis. Apoptosis was first defined in 1972 by Kerr and colleagues, who described this process as a natural form of programmed cell death that is tightly regulated by a variety of environmental stimuli [1]. Molecular mechanisms of apoptosis been extensively discussed in various excellent reviews [2–5]. Apoptosis can be initiated by either the intrinsic pathway or the extrinsic pathway. The intrinsic pathway is triggered by intracellular stressors such as endoplasmatic reticulum (ER) stress, oxidative damage, ischemia, and DNA damage, and

is initiated when cytochrome c is released into the cytosol through channels on the mitochondrial membrane. Mitochondrial outer membrane permeabilization (MOMP) and subsequent release of cytochrome c is regulated by the Bcl-2 family of proteins. When pro-apoptotic signals dominate over anti-apoptotic signals, cytochrome c is released and it forms a complex with the Apaf-1 protein, which is called the apoptosome. The apoptosome cleaves initiator caspase 9 (a cysteine aspartic acid-specific protease), initiating a signaling cascade of protease cleavages that results in the activation of executioner caspases 3, 6 and 7. These executioner caspases induce cell death by cleaving the death substrates, whose cleavage causes critical cellular components to be destroyed.

Alternatively, the extrinsic pathway functions through the activation of death receptors on the cell surface. Upon binding of death ligands such as tumor necrosis factor α (TNFα) or Fas ligand (FasL), the death receptors form a death-inducing signaling complex (DISC) on the cytosolic domain of the receptor. DISC then induces cleavage of initiator caspases 8 and 10, which directly cleave and activate the executioner caspases. This is where the extrinsic and intrinsic pathways converge: the execution phase. Caspases 8 and 10 might also cleave and activate the pro-apoptotic protein Bid, which induces cytochrome C release from the mitochondria. This demonstrates the cross-talk that occurs between the extrinsic and intrinsic pathways [3].

The execution phase is characterized by a series of biochemical and morphological changes to the cell undergoing apoptosis, including chromatin condensation, cell shrinkage, controlled breakdown of cellular protein and DNA. This is followed by fragmentation of the cell into smaller, membrane-enclosed "apoptotic bodies" which are then ingested by phagocytes [4]. One of the defining characteristics of a cell entering the execution phase is the redistribution and externalization of the phospholipid phosphatidylserine (PS) to the outer leaflet of the plasma membrane [5]. "Translocase" is an ATP-dependent enzyme that confines PS to the inner leaflet of the plasma membrane, while the enzyme "floppase" actively pumps cationic phospholipids like phosphatidylcholine (PC) to the outer leaflet [6]. These two enzymes function to maintain this plasma membrane asymmetry between the inner and outer leaflets.

When apoptosis is initiated, translocase and floppase are deactivated and a third ATP-dependent enzyme called "scramblase" undergoes calcium ion-dependent activation. Scramblase is a bidirectional pump that mixes the phospholipids between the inner and outer leaflets, causing a collapse in membrane asymmetry and exposure of PS on the outer membrane that occurs in a matter of minutes. Phagocytes recognize the externalized PS and ingest the apoptotic bodies in an organized manner that does not involve an inflammatory response [7]. PS exposure precedes most of the other biochemical and morphological changes that occur in the apoptosis cascade, making it a marker of early to intermediate apoptosis (Fig. 1).

Apoptosis has an important role in normal processes such as embryonic development, immune system regulation, and tissue homeostasis. However, though it is a tightly regulated process, apoptosis can become dysregulated, resulting in a variety of pathological conditions. Excessive apoptosis can result in a number of neurodegenerative diseases, while insufficient levels of apoptosis can lead to autoimmunity or cancer [8]. Tumor cells often contain mutations that suppress apoptosis and promote cell proliferation so that tumor progression and metastasis can occur. Chemotherapeutic drugs and radiation therapy are common methods of anticancer treatment that usually work by inducing apoptosis in tumor cells. In fact, the effectiveness of these treatments often depends on their ability to induce apoptosis [9, 10]. This is why monitoring apoptosis levels in patients undergoing anticancer treatments could provide very useful information on the status and activity of the disease as well as the efficacy of the therapy.

Current methods of monitoring therapy response involve the use of X-ray Computed Tomography (CT) and Magnetic Resonance Imaging (MRI) to observe changes in the size and morphology of tumors. These methods are not optimal, as it often takes weeks for any observable changes in tumor size to occur, which introduces the possibility for inaccurate assessment of therapy response. It also subjects patients to the unnecessary side effects of ineffective treatments for several weeks, in addition to delaying the initiation of a better, more effective therapy. Non-invasive molecular imaging of apoptosis using single photon emission computed tomography (SPECT) or positron emission tomography (PET) offers a promising solution to this, as it would allow clinicians to assess therapy response in cancer patients immediately following treatment.

Annexin V

The annexins are a superfamily of over 160 proteins that all exhibit calcium-depending binding to anionic phospholipids. They each contain a highly conserved COOH-terminal protein core that contains the Ca^{2+} and membrane binding sites [11]. Annexin V (~ 36 kDa) is a member of this superfamily (Fig. 2), and is expressed in many eukaryotic organisms, including humans. This endogenous protein is mainly present in the cytosol of a variety of different cell types, but can also be found in low concentrations in the blood plasma [12]. It binds selectively with nanomolar affinity to PS, and this binding strongly depends on calcium ion concentration. Bazzi and Nelsestuen [13] found that the amount of annexin V bound to PS

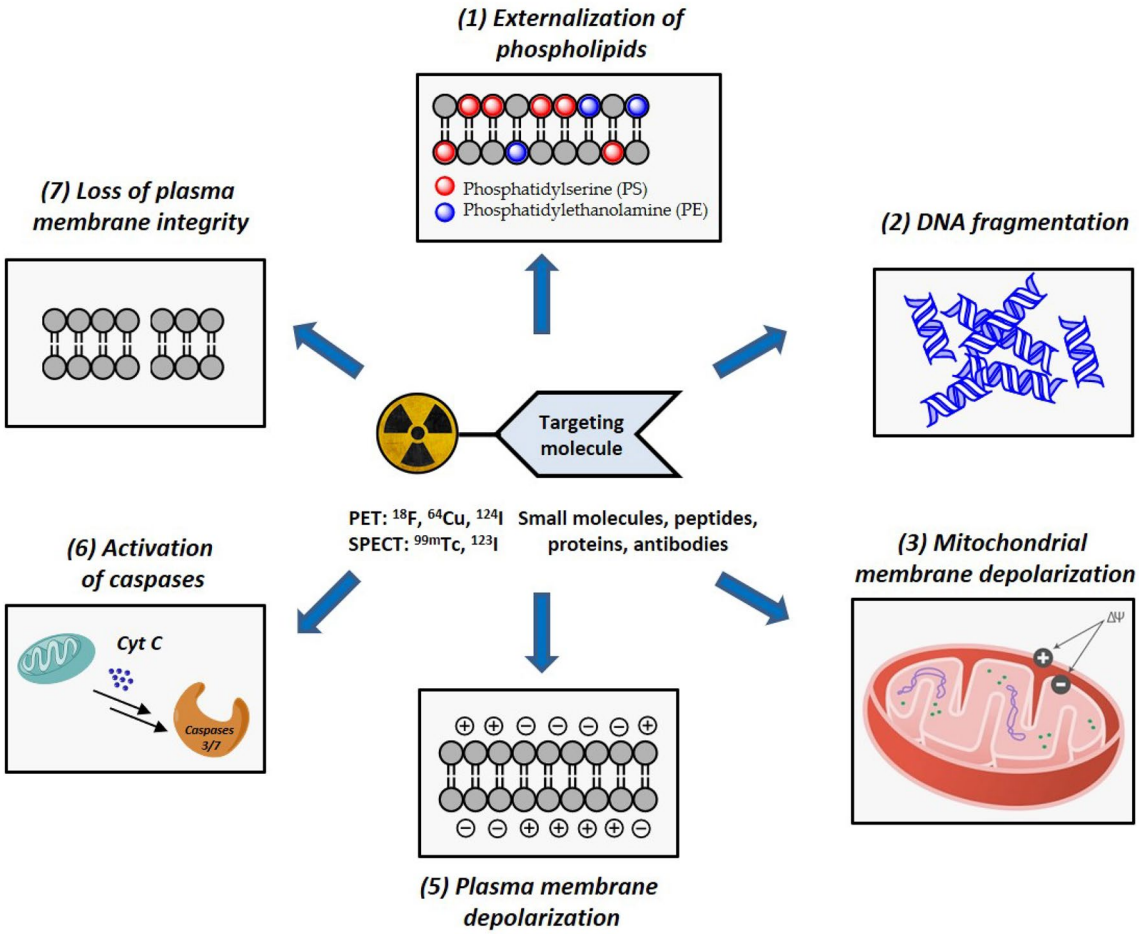

Fig. 1 Targets for molecular imaging cell death

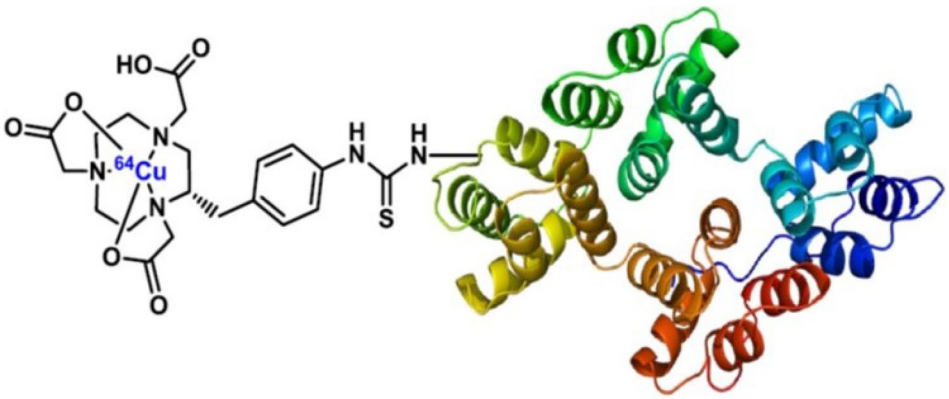

Fig. 2 Structure annexin V labeled with ^{64}Cu through complexation with macrocyclic chelator NOTA [109]

was almost entirely determined by the calcium concentration and unaffected by annexin V concentration. They determined that different calcium concentrations induce different saturation levels of bound annexin V, and that this binding is irreversible upon completion.

The high-affinity binding of annexin V to PS in the presence of physiological levels of calcium makes this protein a sensitive probe for detecting early apoptosis in cells. It is important to note, however, that PS is not exclusively exposed on apoptotic cells; it is also significantly exposed

on necrotic cells and on certain cell types, namely endothelial cells and activated blood platelets [12]. Koopman et al. [14] developed an apoptosis detection assay for cell suspensions that can differentiate between necrotic, apoptotic and viable cells. This assay uses fluorescein isothiocyanate-labeled annexin V (FITC annexin V) to detect apoptotic cells and propidium iodide (PI) to detect necrotic cells using flow cytometry. Although non-invasive molecular imaging techniques utilizing annexin V-PS binding cannot discriminate between different cells with exposed PS, these techniques are essential for in vivo monitoring of apoptosis. Thus, a large amount of research has focused on the development of a clinically suitable form of radiolabeled annexin V.

$^{123/125}$I-labeled annexin V

Though annexin V has been labeled with both ^{123}I and ^{125}I, ^{123}I is the more preferred radionuclide for molecular imaging due to its much shorter half-life (13.2 h) versus the ^{125}I half-life of 59.4 days. Radioiodination of annexin V has been accomplished via both direct and indirect methods. Tait and colleagues used the IodoGen method [15] to directly label annexin V on its tyrosine residues with ^{123}I and ^{125}I, a labeling process also used in the IodoBead method. The IodoGen and IodoBead approaches were then optimized to improve radiochemical yields and purity of ^{123}I-annexin V [16, 17], and a number of studies have shown its usefulness in detecting PS-expressing cells in vitro and in vivo [15, 17–19].

The problem with direct radioiodination is that thyroid hormones have structural similarities to the iodinated residues on annexin V, resulting in rapid in vivo deiodination. In addition to rapid deiodination, clinical biodistribution studies of directly labeled ^{123}I-annexin V showed extensive bowel activity in humans, which precluded imaging of the abdomen [19]. For these reasons, the use of a prosthetic group to indirectly attach radioiodine to annexin V seemed a more suitable alternative. Russell et al. [20] used a Bolton-Hunter reagent (*N*-succinimidyl-3-[^{125}I]iodobenzoate or [^{125}I]SIB) to indirectly label annexin V at its primary amines (lysine residues) with ^{125}I, and compared it to directly-labeled ^{125}I-annexin V (accomplished by the IodoGen and IodoBead methods). Although the in vitro study showed significant PS binding by both the directly and indirectly labeled annexin V in irradiated neuroblastoma cells, the Bolton-Hunter radiotracer showed much greater stability in vivo than the annexin V radioiodinated by the IodoGen / IodoBead methods. The indirectly labeled annexin V also showed significant uptake in apoptotic organs in irradiated mice. Despite these promising features of the Bolton-Hunter radiotracer, its high bowel accumulation, time-consuming production and low radiochemical yields limits its potential for clinical use. The *N*-succinimidyl benzoate molecule has been extensively used in the production of prosthetic groups to indirectly radiolabel annexin V, as it contains an ester that reacts very efficiently with primary amines to form a stable amide bond. Since annexin V contains 21 lysine residues and a terminal primary amine group, labeling with radiolabeled N-succinimidyl benzoates is easy and efficient [21].

^{99m}Tc-labeled annexin V

Most efforts to develop radiolabeled annexin V as a PS-targeting radiotracer have focused on labeling the protein with ^{99m}Tc. This radionuclide is produced by ^{99}Mo/^{99m}Tc generators, and is therefore inexpensive and easily accessible. In addition, its short half-life of 6 h is optimal for SPECT imaging of small molecules, peptides and small proteins, and its low decay energy (0.14 MeV) results in low radiation doses to patients. Together, these desirable characteristics have led to a substantial amount of literature investigating the use of ^{99m}Tc-labeled annexin V in the detection of apoptosis.

^{99m}Tc-BTAP-annexin V

^{99m}Tc-4,5-bis-(thioacetamido)pentanoyl-annexin V (^{99m}Tc-BTAP-annexin V or ^{99m}Tc- N_2S_2-annexin V) was the first ^{99m}Tc-labeled annexin V radioligand to be developed. To produce this radioligand, a ^{99m}Tc-N_2S_2 complex is first formed through a series of steps, and this complex is then attached to annexin V followed by purification, resulting in a product with excellent radiochemical purity. A ^{99m}Tc-BTAP-annexin V formulation kit consisting of 11 components was used by Stratton and colleagues [22] to carry out in vivo evaluations in swine with left atrial thrombi.

This study provided initial evidence that by using radiolabeled annexin V to target PS, in vivo detection of apoptosis using SPECT is possible. In another study, ^{99m}Tc-BTAP-annexin V was injected into patients with atrial fibrillation in order to detect clots [23]. The results of these study showed that ^{99m}Tc-labeled annexin V can be given at safe doses sufficient for clinical imaging. Additional clinical studies have shown that ^{99m}Tc-BTAP-annexin V is effective in the detection of cell death in cardiac allograft patients experiencing transplant rejection [24, 25].

Belhocine and colleagues [26] investigated tumor uptake of ^{99m}Tc-BTAP-annexin V in patients with breast cancer, lung cancer and lymphoma after the first course of chemotherapy. They found a significant relationship between tumor uptake 24–48 h after treatment and patient response to the chemotherapy, which suggested that tumor uptake of ^{99m}Tc-labeled annexin V may be a good predictor of treatment efficacy. However, a clinical study done on the biodistribution and dosimetry of ^{99m}Tc-BTAP-annexin V showed accumulation of this radiotracer in the kidneys, liver and bladder over time as well as fast appearance of activity in the intestines and extensive bowel excretion [27]. This is

a significant limitation, as any imaging of the abdominal region using ^{99m}Tc-BTAP-annexin V would be extremely difficult. Moreover, preparation of the radiotracer is highly complex and time-consuming (even when using the ^{99m}Tc-BTAP-annexin V formulation kit).

Synthesis of ^{99m}Tc-BTAP-annexin V requires rather large starting amount of ^{99m}Tc activity and thus high radiation burden for operators, and results in low radiochemical yields. These limitations make ^{99m}Tc-BTAP-annexin V a poor candidate for clinical use.

^{99m}Tc-I-annexin V

^{99m}Tc-(*N*-1-imino-4-mercaptobutyl)-annexin V (^{99m}Tc-i-annexin V) was developed with the hope that it would address some of the limitations of ^{99m}Tc-BTAP-annexin V. Boersma and colleagues [28] carried out a comparative study between ^{99m}Tc-BTAP-annexin V and ^{99m}Tc-i-annexin V, examining the plasma concentration, excretion and biodistribution patterns of each radiotracer when injected into patients with myocardial disease and various other malignancies. Although ^{99m}Tc-i-annexin V production was fast and easy, it also resulted in a product with low radiochemical purity (lower than ^{99m}Tc-BTAP-annexin V). It also showed slower clearance from the body than ^{99m}Tc-BTAP-annexin V, resulting in much higher radiation doses to most of the organs it accumulated in, including the bladder and the bowel. Its high blood pool activity also severely limited visualization of ^{99m}Tc-i-annexin V uptake by apoptotic or necrotic cells.

^{99m}Tc-HYNIC-annexin V (^{99m}Tc-HYNIC-tricine-annexin V)

Blankenberg et al. [29] radiolabeled annexin V through use of hydrazinonicotinamide (HYNIC), a molecule that is able to sequester ^{99m}Tc. Once the annexin V is randomly labeled with HYNIC on any of its primary amines (lysine residues/terminal amine), this HYNIC-annexin V can be lyophilized and stored indefinitely.

In order to radiolabel it with ^{99m}Tc, the HYNIC-annexin V is reacted with ^{99m}Tc-pertechnetate in the presence of tricine, a co-ligand, at room temperature for 5–10 min. A kit formulation for this radiolabeling procedure is available, and radiolabeling proceeds fast within 15 min to give ^{99m}Tc-HYNIC-annexin V in excellent radiochemical yields > 95%. This simple and efficient labeling procedure made ^{99m}Tc-HYNIC-annexin V a much more promising radiotracer than ^{99m}Tc-BTAP-annexin V for the clinic, and it is consequently one of the most extensively studied and well-characterized apoptosis-detecting radiotracers. Blankenberg and coworkers investigated cell membrane binding of ^{99m}Tc-HYNIC-annexin V compared to FITC-annexin V fluorescence observed via flow cytometry in Jurkat T cell lymphoblasts and ex vivo thymus cell suspensions treated with apoptosis-inducing agents [30]. A linear correlation was found between ^{99m}Tc-HYNIC-annexin V cell membrane binding and FITC-annexin V fluorescence, demonstrating the ability of ^{99m}Tc-HYNIC-annexin V to detect apoptotic cells. They also injected BALB/c mice with ^{99m}Tc-HYNIC-annexin V before and after treatment with anti-Fas antibody, which stimulates hepatocyte apoptosis, and found a threefold increase in hepatic uptake of ^{99m}Tc-HYNIC-annexin V compared to control mice. This suggested that ^{99m}Tc-HYNIC-annexin V was an effective in vivo detector of apoptosis, further confirmed by a histological analysis of the hepatic tissue that showed the presence of hepatocyte apoptosis.

In vivo localization of ^{99m}Tc-HYNIC-annexin V was tested in two other models of apoptosis: acute cardiac allograft rejection in ACI rats and transplanted 38C13 murine B cell lymphomas treated with cyclophosphamide [29]. SPECT imaging showed a significant increase in ^{99m}Tc-HYNIC-annexin V uptake at sites of apoptosis in both of these models. Many other preclinical studies have since demonstrated the effectiveness of ^{99m}Tc-HYNIC-annexin V as a marker for the detection and quantification of apoptosis in vivo. These include animal models of cardiac allograft rejection [31], dexamethasone-induced thymic apoptosis [32], lung transplant rejection [33], liver transplant rejection [34], subacute inflammation [35], cyclophosphamide-induced intramedullary apoptosis [36], autoimmune myocarditis [37], rheumatoid arthritis [38], cardiac ischemia and reperfusion [39], subacute myocarditis [40], cerebral ischemia [41], and chemotherapy- and radiotherapy-treated hepatomas, thymomas, Ehrlich ascites, lymphomas, sarcomas, and breast cancer [42–46].

Considering the preclinical success, ^{99m}Tc-HYNIC-annexin V was further investigated in first-in-human studies via clinical trials. Kemerink et al. [47] carried out a clinical study on the safety, biodistribution and dosimetry of this radiotracer, and established that it was a safe radiotracer for the clinic. It showed greatest uptake in the kidneys, liver and bladder, with predominant urinary excretion and no bowel excretion, making it an excellent candidate for abdominal imaging. However, it concentrates in the cortex of the kidneys, which precludes paranephric imaging.

Nevertheless, many phase II/III clinical trials have demonstrated that ^{99m}Tc-HYNIC-annexin V imaging of tumors and its relationship to response to radiotherapy and/or chemotherapy is a clinically useful radiotracer for non-invasive SPECT imaging of apoptosis.

Clinical studies have also been performed forthe detection of apoptosis in patients with acute myocardial infarction [48], atherosclerotic plaques [49], acute stroke [50, 51], Alzheimer's dementia [52], and head and neck cancer [53, 54]; as well as in patients undergoing preconditioning for ischemia and reperfusion injury [55–57]. Additionally, a

large number of clinical trials have focused on using ^{99m}Tc-HYNIC-annexin V to monitor response of chemo- and radiotherapy in patients with a variety of cancer types [58–62]. These studies demonstrated that ^{99m}Tc-HYNIC-annexin V holds promise to assess apoptosis upon anticancer treatment (Fig. 3).

^{99m}Tc-HYNIC-EDDA-annexin V

Although ^{99m}Tc-HYNIC-annexin V has proven to be a very successful radiotracer for apoptosis detection, its high accumulation in the kidneys is a limitation that others have attempted to address. Decristoforo and Mather [63] investigated the stability of ^{99m}Tc-HYNIC-labeled proteins using either tricine, EDDA, or a ternary tricine/nicotinic acid system as co-ligand, and found that EDDA produced the most stable complex with the most favorable biodistribution in mice. These results inspired Verbeke and colleagues [64] to use EDDA instead of tricine as a co-ligand in the preparation of ^{99m}Tc-HYNIC-annexin V in the hope that this radiotracer would show faster renal excretion and less accumulation of activity in the kidneys. However, their results were disappointing: in mice, ^{99m}Tc-HYNIC-EDDA-annexin V showed no difference in renal excretion compared to ^{99m}Tc-HYNIC-annexin V prepared with tricine, and had even higher accumulation in the kidneys. In addition, ^{99m}Tc-HYNIC-EDDA-annexin V preparation is much more complex and time-consuming than ^{99m}Tc-HYNIC-annexin V, and results in much lower radiochemical yields.

A number of other co-ligands have also been used to label annexin V with ^{99m}Tc-HYNIC in attempts to obtain a radiotracer with more favorable biodistribution characteristics. However, the results from these investigations were similarly disappointing, and tricine remains the best co-ligand for ^{99m}Tc-HYNIC-annexin V production.

^{99m}Tc-MAG$_3$-annexin V

Mercaptoacetyl-glycyl-glycine (MAG$_3$) is a ^{99m}Tc chelator that has been extensively used to radiolabel proteins that often show good renal clearance. It was used to radiolabel annexin V in another attempt to address the high accumulation of activity in the kidney seen in ^{99m}Tc-labeled annexin V [65].

NHS-MAG$_3$ is attached to annexin V in a single reaction step at room temperature, after which the MAG$_3$-annexin V molecule can be labeled with ^{99m}Tc quickly and easily, resulting in very high radiochemical yields (> 90%). The biodistribution study in normal mice showed that kidney and liver uptake of ^{99m}Tc-MAG$_3$-annexin V was significantly reduced compared to ^{99m}Tc-HYNIC-annexin V, and whole body retention of activity was lower as well due to faster clearance. Accumulation of ^{99m}Tc-MAG$_3$-annexin V in the small intestine was sixfold higher than ^{99m}Tc-HYNIC-annexin, which would make abdominal imaging difficult; however, ^{99m}Tc-MAG$_3$-annexin V may be a suitable alternative to ^{99m}Tc-HYNIC-annexin for imaging paranephric structures.

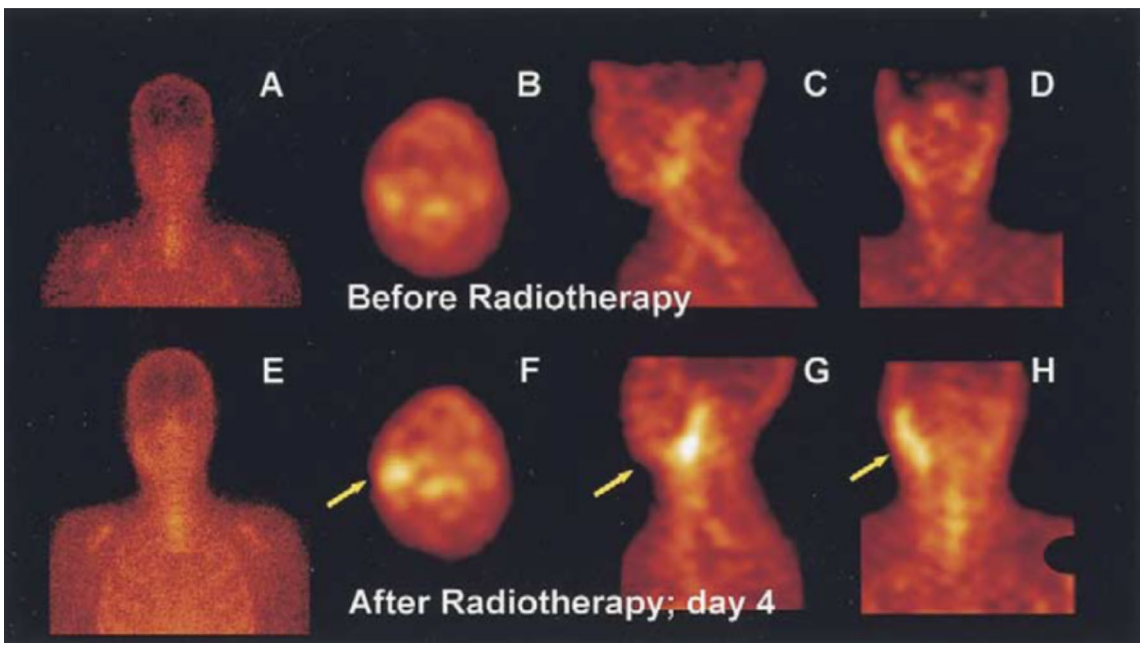

Fig. 3 ^{99m}Tc-annexin V image in a patient with follicular lymphoma grade II before and after radiation therapy (reproduced from Haas et al. [58])

^{99m}Tc-EC-annexin V

Yang and Kim [66] used another ^{99m}Tc chelator, ethylenedicysteine (EC), to radiolabel annexin V with ^{99m}Tc. EC is attached to annexin V in one reaction step, and this conjugate is then subsequently labeled with ^{99m}Tc, resulting in radiochemical yields of almost 100% after gel purification. In vitro cell uptake of ^{99m}Tc-EC-annexin V significantly increased after both radiation and chemotherapy (paclitaxel) treatment. Breast-tumor bearing rats also showed increased tumor uptake of ^{99m}Tc-EC-annexin V 3 days post-treatment, with uptake decreasing to levels lower than those seen in control animals on day 5, possibly due to removal of apoptotic cells by phagocytes. These findings confirm the importance and necessity of choosing the most optimal time for imaging apoptosis after treatment. In a review written by Blankenberg [67], a summary of studies investigating the optimal time for imaging apoptosis post-treatment shows that the highest annexin V uptake occurs within 1–3 days after treatment, which supports the findings of Yang and Kim.

In a clinical study performed on 10 patients with breast cancer, SPECT imaging showed that detectable ^{99m}Tc-EC-annexin V uptake occurred in the tumors of 9 patients, demonstrating the ability of this radiotracer to assess baseline levels of apoptosis in cancer patients [68]. In addition, ^{99m}Tc-EC-annexin V tumor uptake significantly increased in patients who received chemotherapy compared to those who did not, showing that ^{99m}Tc-EC-annexin V would be a useful SPECT radiotracer for detecting treatment-induced apoptosis in order to determine treatment efficacy.

^{99m}Tc- annexin V mutants

Tait and colleagues developed a number of annexin V mutants that contain an N-terminal endogenous chelation site (Ala-Gly-Gly-Cys-Gly-His) for ^{99m}Tc, allowing for direct and site-specific ^{99m}Tc labeling [69]. These mutants had different numbers of calcium binding sites, and with several in vitro and in vivo studies they determined that all four calcium binding sites present on annexin V are necessary for maximal PS binding. In 2006, Tait et al. [70] also demonstrated that using amine-directed modification to randomly label annexin V resulted in significantly reduced membrane binding of apoptotic cells compared to self-chelating annexin V mutants labeled at a single specific site on the N-terminus.

This suggests that random labeling of the 23 amine groups available on annexin V might cause disruption of annexin V-PS binding interactions; a problem that might be addressed with site-specific labeling. With this information, annexin V-128 was developed, which was another mutant that contained the N-terminal Ala-Gly-Gly-Cys-Gly-His ^{99m}Tc chelation site. In vivo studies demonstrated that ^{99m}Tc-annexin V-128 had the same or higher uptake in apoptotic tissues than ^{99m}Tc-HYNIC-annexin V, and had much more favorable biodistribution properties. ^{99m}Tc-annexin V-128 had 88% lower uptake in the kidneys than ^{99m}Tc-HYNIC-annexin V at 60 min post-injection due to faster renal clearance [71].

After seeing such promising results from annexin-V mutants, often referred to as "second generation annexin V", a number of other annexin V variants have been investigated as novel apoptosis imaging agents. Luo and colleagues [72] used ^{99m}Tc-HYNIC to radiolabel annexin B1, an annexin V variant with a slightly longer N terminus that can be produced in large quantities at relatively low cost. This radiotracer showed significantly increased binding to apoptotic cells and tissues compared to controls, and biodistribution studies showed high renal uptake similar to ^{99m}Tc-HYNIC-annexin V. Another group used site-specific mutagenesis to incorporate a single cysteine residue into annexin V, producing cys-annexin V [73]. They used thiol chemistry to modify cys-annexin V using 5-maleimido-2-hydraziniumpyridine hydrochloride (maleimide-HYNIC), so that the incorporated cysteine residue was labeled with HYNIC. The HYNIC moiety could then chelate ^{99m}Tc, resulting in a site-specifically radiolabeled annexin V conjugate. This site-specific thiol-directed labeling using maleimide-HYNIC was meant to eliminate any annexin V-PS binding interference that might occur using amine-directed random labeling with *N*-succinimidyl-HYNIC. The PS-binding abilities of ^{99m}Tc-HYNIC-cys-annexin V were investigated using various murine models of apoptosis, including anti-Fas-induced liver apoptosis, cyclohexamide-induced apoptosis of the liver and spleen, and castration-induced prostate apoptosis. Uptake of ^{99m}Tc-HYNIC-cys-annexin V in apoptotic tissues was significantly higher compared to controls in all of the models except for the castration model, despite histological evidence of prostate apoptosis [73, 74]. This was possible due to the structural organization of prostate cells which provides more of a barrier between the apoptotic prostate cells and circulation.

^{99m}Tc-tricarbonyl-annexin V

Biechlin and colleagues [75] used Traut's reagent 2-iminothiolane (2-IT) to thiol-conjugate annexin V at its lysine residues in order to add a mercaptobutyrimidyl group that could then be radiolabeled with ^{99m}Tc-tricarbonyl $[^{99m}Tc(H_2O)_3(CO)_3]^+$. Although any of the 21 lysines could be thiol-conjugated, the annexin V-SH product had an average of 1 thiol group, similar to the average of 0.9 HYNIC groups found on ^{99m}Tc-HYNIC-annexin V. ^{99m}Tc-tricarbonyl-annexin V showed similar binding to apoptotic tissues

compared to ^{99m}Tc-HYNIC-annexin V, but the radiolabeling yields for ^{99m}Tc-tricarbonyl-annexin V were better.

Using 2-IT instead of HYNIC to label annexin V with ^{99m}Tc appeared to provide a more stable labeling method, with fewer possible isomeric products than seen with ^{99m}Tc-HYNIC-annexin V in biological models. Another possible advantage could be that 2-IT can be purchased and used without purification, while the HYNIC prosthetic group must be chemically synthesized.

Since the ^{99m}Tc-tricarbonyl ion targets histidine residues in addition to cysteine residues, his-annexin V (annexin V with an N-terminal histidine tag) was used by Vangestel et al. [76] in order to site-specifically label the protein with ^{99m}Tc-tricarbonyl at the histidine residue, away from the binding regions of the protein to prevent any PS binding disruptions. ^{99m}Tc-tricarbonyl-his-annexin V was produced in yields of 70–85%, and in vitro studies using colorectal cancer cells treated with the apoptosis-inducing agent 5-FU showed that this annexin V conjugate fully retained its PS-binding activity. Colorectal tumor-bearing mice were used to image spontaneous apoptosis levels in vivo, showing significant tracer binding in apoptotic tissues, with rapid blood clearance and highest uptake in the kidneys and liver.

Another group carried out a comparative study between three different types of ^{99m}Tc-labeled second generation annexin V (cys-annexin V): ^{99m}Tc-tricarbonyl-his-cys-annexin V, ^{99m}Tc-HYNIC-cys-AnxV, and ^{99m}Tc-tricarbonyl-DTPA-cys-AnxV [77]. In vitro PS-binding studies were done on Jurkat T-lymphocyte cells treated with ionomycin as an apoptosis-inducing agent, biodistribution studies were carried out in healthy mice, and a Fas-mediated hepatic model of apoptosis was used to investigate these three radiotracers in vivo. These studies showed that ^{99m}Tc-tricarbonyl-labeled cys-annexin V has better radiolabeling yields, stability, biodistribution and affinity for apoptotic tissues in vivo than ^{99m}Tc-HYNIC-labeled cys-annexin V. ^{99m}Tc-tricarbonyl-his-cys-annexin V had the fastest blood clearance and urinary excretion, and also showed significantly lower liver uptake than the other two tracers.

^{111}In-labeled annexin V

With a long half-life of 2.81 days and low gamma energies of 0.171 and 0.245 MeV, it was thought that ^{111}In might also be a suitable SPECT radionuclide to label annexin V for the detection of apoptosis, as it would allow for prolonged diagnostic scanning protocols over the course of days, while maintaining a low radiation dose in patients. Wen and colleagues [78] labeled annexin V with polyethyleneglycol (PEG), after which diethylenetriamine-pentaacetic acid (DTPA), an ^{111}In chelator, was attached to the PEGylated annexin V. The DTPA-PEG-annexin V was radiolabeled with ^{111}In, achieving yields of about 92% with high radiochemical purity.

Mammary tumor-bearing mice were treated with either Paclitaxel or anti-EGR MoAb to induce apoptosis, and tumor uptake of ^{111}In- DTPA-PEG-annexin V correlated well with apoptotic levels determined by histological analysis. Enhanced contrast in the tumors could be seen 48 h after radiotracer injection, which suggests that a longer circulation time for annexin V radiotracers might improve visualization of apoptotic tissue.

^{124}I-labeled annexin V

^{124}I has a relatively long half-life of 4.18 days, which would allow for labeling procedures of longer duration, and would also make this radionuclide more easily distributed. However, it could also mean higher radiation doses to any organs that it accumulates in when injected into patients. Its low ratio of disintegrations (26% positron emission, 74% electron capture) also results in fewer positrons and thus a smaller PET signal, which could mean that higher injected doses are needed.

Similar to $^{123/125}$I, annexin V has been radiolabeled with ^{124}I via both direct and indirect methods. Glaser and colleagues [79] directly iodinated annexin V using the chloramine-T method to make ^{124}I-annexin V. They indirectly labeled annexin V using the pre-labeled *N*-succinimidyl-3-[^{124}I]iodo-benzoate ([^{124}I]m-SIB) reagent to produce [^{124}I]m-IBA-annexin V, or [^{124}I]SIB-annexin V, in a three-step procedure. Both the indirect and direct labeling methods resulted in low radiochemical yields, and the specific activity of [^{124}I]m-IBA-annexin V was ninefold lower than that of ^{124}I-annexin V. The two radiotracers showed similar PS binding in HL60 human leukemia cells, with increased binding in cells treated with the apoptosis-inducing agent camptothecin. However, not all of these increases were statistically significant, and the model used was not suitable to accurately assess apoptosis levels. Collingridge et al. [80] found that in mice with 5-FU-treated RIF-1 tumors, [^{124}I]SIB-annexin V failed to detect apoptosis, and it accumulated in the kidneys and bladder.

Dekker and Keen et al. [81, 82] used a similar method to indirectly label annexin V with ^{124}I, but used [^{124}I]*N*-hydroxysuccinimidyl-4-iodobenzoate as the reagent in order to prepare [^{124}I]4IB-annexin V, also achieving rather low radiochemical yields. They carried out a comparative study between [^{124}I]4IB-annexin V and directly labeled ^{124}I-annexin V, and found that in Jurkat cells, the PS-binding rate of [^{124}I]4IB-annexin V was faster. In addition, both radioligands showed significant increases in membrane binding in cells treated with camptothecin. In a mouse model of hepatic apoptosis, injection of anti-Fas antibody induced significantly higher hepatic uptake of both

radiotracers, which correlated well with ex vivo histological analyses of apoptosis levels. However, this difference in uptake between treated and untreated mice was greater for ^{124}I-annexin V. The biodistribution study showed that [^{124}I]4IB-annexin V was more stable in plasma and accumulated in the kidney, while ^{124}I-annexin V accumulated in the stomach and thyroid.

^{124}I-MBP-annexin V

Dekker and Keen et al. [83] later developed ^{124}I-maltose-binding protein-annexin V (^{124}I-MBP-annexin V), whereby MBP-annexin V is first produced, and this chimera is later directly iodinated via the IodoGen method. ^{124}I-MBP-annexin V showed significantly higher binding to camptothecin-treated Jurkat cells compared to control cells.

In a mouse model of liver apoptosis, ^{124}I-MBP-annexin V exhibited liver uptake that was nine times greater in mice treated with anti-Fas antibody than in untreated mice, and histological analysis of the liver tissues confirmed the presence of apoptotic hepatocytes in anti-Fas-treated mice. However, biodistribution of ^{124}I-MBP-annexin V showed high accumulation of activity in the thyroid, representative of rapid dehalogenation. Thus, the use of a prosthetic group to label MBP-annexin V with ^{124}I might be more suitable in order to prevent dehalogenation, which seems to be characteristic of direct iodination methods.

^{18}F-labeled annexin V

Although a cyclotron is required for its production, ^{18}F is an attractive radionuclide for molecular imaging as it can be produced in very large amounts with high specific activity, and its short half-life of 109.8 min results in lower radiation doses in patients compared to ^{99m}Tc ($t_{1/2} = 6$ h). Its low positron energy of 0.64 MeV and rapid urinary excretion also contribute to lower radiation doses. The radiation properties of ^{18}F are excellent for PET imaging, since 97% of its radiation is from positron emission, with the remaining 3% from electron capture.

[^{18}F]SFB-annexin V

Several studies have described a four-step synthesis similar to that used for the production of [^{124}I]m-IBA-annexin V that uses *N*-succinimidyl-4-[^{18}F]fluorobenzoate ([^{18}F]SFB) as a precursor in order to produce 4-[^{18}F]fluorobenzoyl-annexin V, also referred to as [^{18}F]SFB-annexin V. In 2003, Zijlstra and colleagues [84] developed an automated synthesis module for [^{18}F]SFB-annexin V production, allowing for much greater starting activities and radiochemical yields of about 20% with purities of at least 95%. Although yields were not very high, the automated synthesis module produced large batches of the product. This radiotracer showed 60% increased binding to apoptotic Jurkat T-cell lymphoblasts (induced by irradiation) compared to non-apoptotic control cells.

Toretsky and colleagues [85] used a greater annexin V concentration of 5 mg/mL (Zijlstra et al. had used 3 mg/mL) in the production of [^{18}F]SFB-annexin V, resulting in much higher yields of up to 70%. TC32 sarcoma cells treated with the apoptosis-inducing agent etoposide showed 88% higher binding of [^{18}F]SFB-annexin V compared to untreated cells, which correlated well with FITC-annexin V apoptosis quantification. This showed that conjugation of annexin V with [^{18}F]SFB does not reduce its ability to bind to apoptotic cells.

Grierson et al. [86] further optimized [^{18}F]SFB-annexin V production by investigating the use of varying amounts of annexin V and precursor as well as different reaction times. Using even higher annexin V concentrations, they were able to obtain yields of 77%; however, under the most favorable and practical conditions, they obtained yields of 64%. A cell binding assay done on PS-expressing red blood cells demonstrated that [^{18}F]SFB-annexin V PS-binding activity remained intact.

In addition, a pilot PET biodistribution study was done on normal Sprague–Dawley rats, showing highest [^{18}F]SFB-annexin V uptake in the kidneys and bladder and rapid clearance from the other organs. [^{18}F]SFB-annexin V was also produced by Murakami and colleagues [87], who carried out a 2 h manual synthesis instead of using an automated synthesis module using relatively low amount of annexin V (0.1 mg, 2 mg/mL).

These conditions might explain the very low yields they obtained (10%). This group also produced ^{99m}Tc-mutant annexin V using the self-chelating mutant annexin V-117 in order to carry out a comparative study between ^{18}F-labeled annexin V and ^{99m}Tc-labeled annexin V. An ex vivo imaging study was done on Wistar rats, whereby each radiotracer was injected into a rat 24 h after the induction of myocardial ischemia in the left ventricle. Both radiotracers showed a threefold increase in uptake in the left ventricle in ischemic rats compared to control rats, and they showed a similar heart to blood activity ratio in normal rats. However, the biodistribution in normal rats showed significantly lower accumulation of [^{18}F]SFB-annexin V in the liver, spleen and kidneys than ^{99m}Tc-mutant annexin V, suggesting that ^{18}F-labeled annexin V may be more suitable for use in the clinic.

In 2005, Yagle et al. [88] carried out another preclinical PET imaging study in a rat model of apoptosis using [^{18}F]SFB-annexin V as a radiotracer. Rats were treated with cyclohexamide to induce liver apoptosis, which caused a 3 to ninefold increase in liver uptake of [^{18}F]SFB-annexin V compared to control rats. Histological analyses of the liver

tissue confirmed that uptake correlated well with apoptosis levels. [^{18}F]SFB-annexin V was rapidly cleared from the blood and excreted in the urine, which resulted in high image contrast between healthy and apoptotic/necrotic tissues. This demonstrates an advantage of [^{18}F]SFB-annexin V over ^{99m}Tc-labeled annexin V, which tends to show accumulation in the kidneys and slow excretion.

Recently, [^{18}F]SFB-annexin V was investigated in a tumor model of chemotherapy-induced apoptosis [89]. Mice with human head and neck squamous cell cancer UM-SCC-22B tumor xenografts were treated with two doses of doxorubicin with a 1 day interval, and PET imaging of the mice was done at 6 h and 24 h as well as 3 and 7 days post treatment. They found that tumor uptake began to increase at the earliest time point and peaked at 3 days post treatment, with uptake values significantly higher than those seen in control (untreated) tumors. This significantly higher uptake at day 3 was not accompanied by changes in tumor size, suggesting that radiotracer uptake precedes tumor reduction. Difference in uptake between treated and control tumors disappeared by day 7, but reduction in tumor size could often be seen at this point.

[^{18}F]SFB- and [^{18}F]FBEM-annexin V

Perreault et al. [90] have recently described random and site-specific labeling of annexin V with [^{18}F]SFB as amine-reactive group and *N*-[2-(4-[^{18}F]fluorobenzamido)ethyl]maleimide [^{18}F]FBEM as thiol-reactive prosthetic group (Fig. 4).

The authors examined both bioconjugation methods on PS-binding ability of ^{18}F-labeled annexin V in camptothecin-treated EL4 cells.

While site-specific radiolabeling used only very low amounts of protein (~0.1 mg), achieved radiochemical yields were only moderate (4–9%). When compared with the well-characterized, randomly labeled [^{18}F]SFB-annexin V, site-specific labeled [^{18}F]FBEM-annexin V showed no difference in the ability to detect apoptotic cells.

Its binding to camptothecin-treated EL4 cells was comparable and therefore it was concluded that more complex site-specific labeling of annexin V may not of advantage compared to the simpler and more economical random radiolabeling technique [90].

[^{18}F]FBABM-annexin V-128

[^{18}F]SFB-annexin V showed good biodistribution in animals and was demonstrated to be a very effective PET radiotracer for the detection of apoptosis. However, since the prosthetic group [^{18}F]SFB can conjugate to any of the 23 primary amines present on annexin V, this non-specific, amine-directed conjugation of annexin V might affect the PS-binding properties of the protein, as was shown by Tait and colleagues [71]. Radiolabeling methods that target the free thiol group of the single cysteine residue present on wild-type annexin V can be used as a more site-specific labeling approach, which can be accomplished with thiol-reactive groups such as *N*-substituted maleimides instead used the mutant annexin V-128, which contains a more easily accessible cysteine on its N-terminal region [91]. They labeled the thiol group on the N-terminal cysteine of annexin V-128 with *N*-[4-[(4-[^{18}F]fluorobenzylidene) aminooxy] butyl]maleimide ([^{18}F]FBABM) in a two-step, one-pot reaction, obtaining a 37% radiochemical yield with > 98% purity. They also labeled wild-type annexin V on its single endogenous thiol group with [^{18}F]FBABM to use as a negative control, but could only obtain yields of less than 0.2%, demonstrating the difficulty in targeting this internal cysteine.

In a calcium-titrated cell binding study done on red blood cells with exposed PS, membrane binding of [^{18}F]FBABM-annexin V-128 was comparable to that seen by wild type annexin.

[^{18}F]FDG-MHO-annexin V

Wuest et al. [92] also used a site-specific, thiol-targeted approach to label the single internal cysteine on wild-type

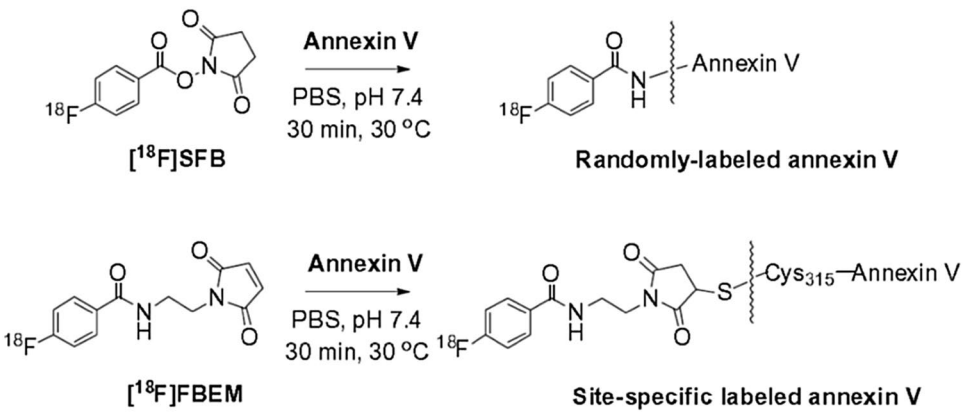

Fig. 4 Random and site-specific labeling of annexin V with [^{18}F]SFB and [^{18}F]FBEM (reproduced from Perreault et al. [90])

annexin V. Here 2-[^{18}F]Fluoro-2-deoxy-D-glucose ([^{18}F]FDG), the most commonly used and widely available PET tracer, was used as a building block for the synthesis of the prosthetic group [^{18}F]FDG-maleimidehexyloxime ([^{18}F]FDG-MHO), which was then conjugated to annexin V. To produce the [^{18}F]FDG-MHO, readily available [^{18}F]FDG was reacted with aminooxymaleimide hydrochloride for 15 min at 100 °C, after which the product underwent solid-phase extraction and was then purified by HPLC. This took a total of 45 min. The [^{18}F]FDG-MHO was then directly added to annexin V (100 µL, 1.0 mg/mL) and incubated at room temperature for 30 min. After size-exclusion purification, [^{18}F]FDG-MHO-annexin V yields of 43–58% were obtained, which is surprisingly high compared to the yields of endogenous thiol-labeled annexin V obtained by Li et al. [91].

[^{18}F]SFB-annexin B1

Very recently, Wang and colleagues [93] used second generation annexin V (annexin B1) radiolabeled with [^{18}F]SFB for PET imaging of apoptosis. They obtained a radiolabeling yield of 20% in 40 min, and [^{18}F]SFB-annexin B1 showed significantly higher binding in Jurkat cells treated with anti-Fas antibody compared to control cells. PET/CT studies were done using normal rats, which showed highest uptake in the liver and kidneys like most other annexin V radiotracers, and rats with W256 breast tumors showed much higher tumor uptake when treated with cyclophosphamide compared to those that did not receive chemotherapeutic treatment. This group also investigated [^{18}F]SFB-annexin B1 uptake in rabbits with ischemia-reperfusion-induced apoptosis in the right kidney. At 2 h post-injection, they found an indistinguishable accumulation in both the ischemic kidney and the normal left kidney, suggesting that the high renal clearance and accumulation of this radiotracer in vivo precludes its utility in PET imaging of renal structures. However, at 4 h post-injection, the ischemic right kidney showed significantly higher retention of [^{18}F]SFB-annexin B1, and uptake in the left kidney had decreased significantly.

^{64}Cu-labeled annexin V

In 2007, Cauchon et al. [94] utilized the extremely high binding affinity of streptavidin (SAv) for biotin to develop a new method of PET imaging of apoptosis using annexin V. In order to radiolabel SAv with ^{64}Cu, they first coupled DOTA (1,4,7,10-tetraazacyclododecane-N,N',N'',N'''-tetraacetic acid), a well-characterized ^{64}Cu chelator, to biotin, and then reacted this ^{64}Cu-DOTA-biotin molecule with an excess of SAv to produce ^{64}Cu-DOTA-biotin-SAv.

SAv is a tetramer that contains four biotin binding sites, so they loaded it with sevenfold less ^{64}Cu-DOTA-biotin than is needed for saturation in order to only attach one ^{64}Cu-DOTA-biotin molecule to each SAv. This left 3 more biotin binding sites available on the SAv, so that ^{64}Cu-DOTA-biotin-SAv could then bind to biotinylated annexin V.

Production of ^{64}Cu-DOTA-biotin-SAv took about 2 h and resulted in > 70% yields, depending on ^{64}Cu content. In vivo PET studies were carried out using EMT6 mammary tumor-bearing BALB/c mice treated with photodynamic therapy (PDT) in order to investigate the efficacy of ^{64}Cu-DOTA-biotin-SAv in detecting PS-bound biotinylated annexin V. The mice were first injected with biotinylated annexin V, followed by an avidin injection 2 h later in order to eliminate free biotinylated products, followed by a final injection of ^{64}Cu-DOTA-biotin-SAv a further 2 h after the avidin chase. PET imaging showed increased tumor uptake of ^{64}Cu-DOTA-biotin-SAv in PDT-treated mice compared to control mice, which correlated well with ex vivo histological analyses of tumor apoptosis levels. In vitro studies with EMT6 cells also showed significantly higher ^{64}Cu-DOTA-biotin-SAv uptake when treated with PDT. However, ^{64}Cu is not among the most suitable radionuclides for clinical PET imaging, since most of its radioactivity is from electron capture and beta decay, with only 20% positron emission.

On the other hand, substitution of ^{64}Cu for ^{61}Cu ($t_{1/2}$=3.4 h, 62% positron emission) in this method may provide a good alternative. In addition, timing between each of the three different injections must be optimized.

^{68}Ga-labeled annexin V

^{68}Ga has a half-life of 67.7 min, and this positron-emitter is conveniently available through ^{68}Ge/^{68}Ga generators. Since attempts to label annexin V with ^{18}F have resulted in rather low radiochemical yields and ^{18}F radiochemistry relies on cyclotrons, it was thought that ^{68}Ga-labeled annexin V might be a better alternative. Bauwens et al. [95] used ^{68}Ga-Dotamaleimide to site-specifically label two annexin V mutants, Cys2-annexin V and Cys165-annexin V, which contain a single cysteine residue at the 2-position and the 165-position, respectively. Total synthesis of ^{68}Ga-Cys2-annexin V and ^{68}Ga-Cys165-annexin V took 55 min, and both were produced in yields of about 25% (43% decay-corrected) with purities around 98%. Apoptosis was induced in vitro and in vivo using anti-Fas treatment, and found that treated Jurkat cells bound 5 times more ^{68}Ga-Cys2-annexin V and ^{68}Ga-Cys165-annexin V than untreated cells, and that normal mice treated with anti-Fas showed greater hepatic uptake of the tracer than untreated mice. When the radiotracers were injected into mice inoculated with lymphoma cells, baseline tumor uptake was extremely low and PET-MRI fusion images were required in order to delineate the tumor images.

However, tumor uptake greatly increased after the mice were treated with a combination of chemotherapy and radiation therapy. Biodistribution of ^{68}Ga-Cys2-annexin V and ^{68}Ga-Cys165-annexin V showed high liver uptake and kidney retention, similar to many other radiolabeled annexin V analogues.

There is an abundance of literature on the radiolabeling of annexin V for PET and SPECT imaging of apoptosis, which would have many clinical uses, particularly the assessment of chemotherapy response in cancer patients. Although many different radionuclides and prosthetic groups have been used to radiolabel annexin V, ^{99m}Tc-HYNIC-annexin V is the only annexin V radioligand to have reached clinical trials thus far. Since ^{99m}Tc-HYNIC-annexin V has such high accumulation in the kidneys and liver, it would be beneficial to find a more suitable radiotracer to be used in humans. Additionally, since PET is a more sensitive and quantitative imaging method than SPECT, substantial research has gone into the development of an annexin V PET radiotracer for clinical use, with emphasis on ^{18}F-labeled annexin V due to the desirability of this radionuclide's properties.

Synaptotagmin I

The C2A domain of synaptotagmin I is a 14.7 kDa protein, which like annexin V binds to PS in a Ca^{2+}-dependent manner [96]. A glutathione-S-transferase (GST)-tagged version of C2A was shown to detect cell death in vitro and in vivo using radionuclide and MR imaging techniques [97].

The protein is of interest since, due to its smaller size, it would likely exhibit better penetration of tumor tissue than annexin V, better clearance of unbound material, and, as a result, better tumor tissue contrast [98]. C2A(S78C)-Alexa Fluor 647 showed lower binding to viable cells than a derivative of annexin V carrying the same fluorescent tag, and therefore better specificity to detect apoptotic EL4 cells treated with etoposide [98]. It was concluded that the lower binding to viable cells may be important to reduce non-specific tissue accumulation compared to radiolabeled annexin V derivatives. Since several lysine residues in this protein are critical for PS binding, Tavare et al. [99] engineered a new protein, C2AcH, to include the C-terminal sequence CKLAAALEHHHHHH, incorporating a free cysteine (for site-specific covalent modification) and a hexahistidine tag (for site-specific radiolabeling with $[^{99m}Tc(CO)_3(OH_2)_3]^+$). They also engineered a second derivative, C2Ac, in which the C-terminal sequence included only the C-terminal cysteine. The authors found that site-specifically labeled C2AcH exhibited calcium-dependent binding to the PS on the RBC, whereas a nonspecifically modified derivative, C2AcH-B, in which lysines had been modified with benzyloxycarbonyloxy, did not. They concluded that Cys and a His-tag enhanced the rate and efficiency of labeling with $[^{99m}Tc(CO)_3(OH_2)_3]^+$ compared to either the His-tag or the Cys alone, and that this sequence would be suitable for further evaluation as a radiolabeling tag. Non-site-specific modification of C2A via lysine residues seemed to impair PS target binding affinity and ^{99m}Tc-C2AcH had excellent radiolabeling, stability and PS binding characteristics which would be of interest for evaluation in vivo [99].

Follow-up studies from the same research team have reported labeling with ^{68}Ga as well as ^{64}Cu [100]. Since the calcium binding sites in C2A may interfere with copper binding, the authors were searching for a high affinity, fast labelling chelator.

They choose a maleimide-functionalized bis(thiosemicarbazone), H2ATSE/AMal, for the site-specific copper-64 radiolabeling of thiol-functionalized C2Ac. During radiolabeling by incubation of the ligand–protein conjugate with $[^{64}Cu]Cu^{2+}$, analysis of the final labeling complex ^{64}CuATSE/AMal-C2Ac revealed that the C2Ac competed for $^{64}Cu^{2+}$ with the chelator. In contrast, when pre-labeling ^{64}CuATSE/AMal and then conjugating it to C2Ac the final product showed good stability in serum and maintained PS affinity in a red blood cell binding assay [100]. These findings suggested that due to the intrinsic copper binding properties of the protein, a pre-labelling approach is preferred for the C2Ac domain of synaptotagmin I when labeling it with ^{64}Cu [100]. However, none of these radiometal-labeled synaptotagmin I derivatives were evaluated in vivo, therefore a final conclusion on their suitability as in vivo imaging agents cannot be drawn from these studies. However, parallel work from Wang et al. [101] has led to a ^{18}F-labeled C2A-glutathione-S-transferase (GST). Labeling with ^{18}F was achieved through bioconjugation with prosthetic group ^{18}F-SFB. The binding of ^{18}F-C2A-GST to PS on apoptosis-induced cells in vitro was validated using camptothecin-induced Jurkat cells resulting in a fourfold increased binding. Single-dose paclitaxel treatment was used to induce apoptosis in rabbits bearing VX2 tumors.

Uptake of ^{18}F-C2A-GST in VX2 tumors increased from SUV_{max} 0.009 (control) to 0.47 after paclitaxel treatment [101]. However, these values seem to be very small and would need further validation. A more recent analysis by Neves et al. [102] evaluated a near-infrared fluorophore-labeled and ^{99m}Tc- and ^{111}In-labeled derivatives of C2Am for imaging tumor cell death, using planar near-infrared fluorescence imaging and SPECT in implanted and genetically engineered mouse models of lymphoma and in human colorectal xenografts. They demonstrated the capability of C2Am to detect tumor cell death in vivo as early as 2 h after administration. The authors had generated a smaller C2A domain of only 16 kDa size for a potential better tissue penetration and clearance and introduced a site-directed mutation (S78C; C2Am) that allowed for site-specific labeling [102].

Radiolabeled C2Am derivatives showed favorable biodistribution profiles, with predominantly renal clearance, and there was a close correlation between C2Am binding and histologic markers of cell death [102].

Phosphatidylserine-binding peptides

There are several challenges associated with the use of radiolabeled annexin V for in vivo imaging of cell death, which have limited its use in the clinic. These challenges include elaborate and complex radiolabeling procedures, poor biodistribution profiles displaying high nonspecific uptake into the liver and kidneys, slow blood clearance resulting in poor image contrast, inability to control Ca^{2+} concentrations in vivo, poor tumor tissue penetration, and lack of knowledge of the optimal time for imaging after cell death has been induced and radiolabeled annexin V has been administered. Therefore, alternative strategies and concepts for the development of PS-binding radiotracers are needed.

Peptides represent an alternative and promising strategy to target PS. They provide several advantages over annexin V including better pharmacokinetics due to their smaller size, better availability, and simpler synthesis and radiolabeling strategies [103]. To identify lead peptide structures binding against PS, phage-display [104] or combinatorial cell screen approaches were utilized [105]. Burtea et al. have described various small PS-binding peptides which were identified through phage display screening [104]. The determined IC_{50} values to compete with annexin-V for PS binding were in the range of 10 to 15 mM for hexapeptides PGDLSR and LIPPKF. Initial evaluation in vitro and in vivo in apoptosis models used Gd-DTPA-g-LIKKPF as PS targeting compound. However, the reported inherent low sensitivity of metal complex Gd-DTPA-g-LIKKPF seems to be a major limitation for its application as MRI imaging agent of PS in apoptosis [104]. Another study utilizing phage display to generate PS-binding peptide structure PS3-10 has extensively discussed structure-related key amino acids essential for binding to PS [106].

^{18}F-labeled PGDLSR and LIPPKF

Small peptides can easily be labeled with short-lived positron emitter ^{18}F using prosthetic group bioconjugation chemistry [107]. Typical and frequently employed examples are acylating agent *N*-succinimidyl-4-[^{18}F]fluorobenzoate ([^{18}F]SFB) and alkylating agent *N*-[6-(4-[^{18}F]fluorobenzylidene) aminooxyhexyl]-maleimide ([^{18}F]FBAM). Both peptide sequences PGDLSR and LIPPKF, which were identified by Burtea et al. [104] as lead PS-binding peptide structures, were successfully labeled with [^{18}F]SFB and [^{18}F]FBAM (Fig. 5) [108].

The latter case used *N*-terminal cysteine-containing peptides CPGDLSR and CLIPPKF for radiolabeling with [^{18}F]FBAM. Radiolabeling of peptides with [^{18}F]FBAM proceeded chemoselectively at the cysteine residue in higher radiochemical yields compared to radiolabeling with [^{18}F]SFB. For evaluation of these ^{18}F-labeled small linear peptides targeting PS a novel competitive radiometric PS binding assay using ^{64}Cu-labeled NOTA-annexin V as radiotracer was developed [109]. In this binding assay PS was immobilized and competitive binding of ^{64}Cu-labeled NOTA-annexin V was measured in the presence of novel

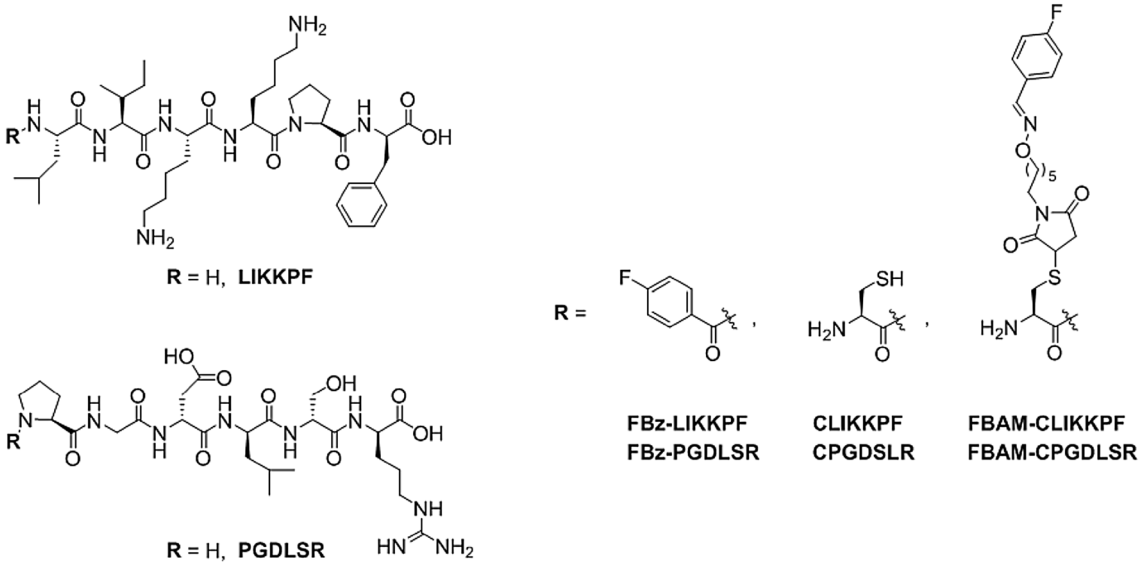

Fig. 5 Structures of LIKKPF and PDGLSR and their FBz and FBAM derivatives as used for ^{18}F-labeling (reproduced from Wuest et al. [109])

peptide structures and compared to unlabeled annexin V for direct comparison. A radiometric binding assay seems to be the most accurate way to determine target protein binding of compounds under investigation. Competition of both linear peptides LIKKPF and PGDLSR against ^{64}Cu-labeled NOTA-annexin V, and our assay revealed that both peptides displayed about four to five orders of magnitude lower IC_{50} values (mM range) compared to wild-type annexin V (nM range).

This was in contrast to the findings of Burtea et al. [104] who reported both peptides binding in the nanomolar range. An independent analysis of their fluorescence labeled derivatives in a fluorescence-based assay revealed K_d values also in the micromolar range [110].The discrepancy in the determined IC_{50} values may result from different sensitivities of the detection methods used in the PS-immobilized in vitro assay. While Burtea et al. [104] performed a staining reaction between horse-radish-peroxidase (HRP)-conjugated streptavidin and biotinylated annexin V, the radiometric assay used PS-bound ^{64}Cu-labeled NOTA-annexin V directly [109].

The latter assay clearly demonstrated that the small peptide structures LIKKPF and PGDLSR as well as their derivatives FBz-LIKKPF, FBz-PGDLSR, FBAM-CLIKKPF and FBAM-CPGDLSR are significantly less potent (IC_{50} values in the low mM range) to interact with PS compared to wild-type annexin V (IC_{50} value in nM range). In addition to these findings, the in vivo stability of these compounds was also very poor. While [^{18}F]FBAM-CLIKKPF was found to be slightly more stable (~25% intact after 15 min) [^{18}F]FBAM-CPGDLSR was completely metabolized [109].

Despite that, increased binding of [^{18}F]FBAM-CLIKKPF to apoptotic Jurkat cells was detected in vitro revealing some interaction and binding to PS. However, increased uptake in an apoptotic in vivo model was not shown [110]. Taken together, both small linear peptide sequences LIKKPF and PGDLSR exhibited poor performance as PET imaging peptides in vivo as discussed above. LIKKPF was labeled with ^{18}F through bioconjugation chemistry with [^{18}F]FDG, but resulting radiopeptide was not successful in PET imaging of PS in apoptotic tumors [111]. A recent addition to the study of these hexapeptides was carried out by Azzouna et al. by labeling PGDLSR with ^{68}Ga and ^{67}Ga via conjugating β-alanine-NODAGA to the N-terminus [105]. Competition binding against biotinylated annexin V in an enzyme-linked immune-absorbent ELISA assay yielded IC_{50} values of 131 nM for PDGLSR and 185 nM for ^{nat}Ga-NODAGA-β-alanine-PDGLSR. These finding are inconsistent with values determined by Wuest et al. [109] but may be caused by the use of different in vitro assays. Azzouna et al. also found that ^{67}Ga-NODAGA-β-alanine-PDGLSR was stable in human serum in the presence of metalloprotease inhibitor phenanthronine monohydrate in vitro up to 60 min [112]. However, no analysis on in vivo metabolic stability was reported. In a SPECT imaging experiment involving a rat model of infective endocartitis,the authors detected no focal uptake of ^{67}Ga-NODAGA-β-alanine-PDGLSR in the area of the heart using SPECT but did point out a localization of this compound in vegetations on aorta root and aorta valve. The in vivo experiments were carried out in the absence of metalloprotease inhibitor and thus together with findings from Wuest et al. [109] did indirectly confirm that PGDLSR is not metabolically stable in vivo and therefore not suitable for further development as a molecular imaging agent for apoptosis.

^{64}Cu-labeled PSBP-6 versus ^{99m}Tc-labeled SAAC-PSBP-6

PSBP-6, a 14-mer PS-binding peptide 6 (FNFRLKAGAKIRFG, PSBP-6), reported by Xiong et al. [113], is a modified version of the synthetic 14-mer peptide PSBP-0 (sequence FNFRLKAGQKIRFG) originally identified and described by Igarashi et al. in 1995 [113]. PSBP-0 was derived from a conserved PS-specific binding site found on protein kinase C and PS decarboxylase, an enzyme that converts PS to phosphatidylethanolamine (PE) [114]. PSBP-0 was found to bind specifically to PS, but with low affinity. Xiong et al .later produced a library of 14-mer peptides based on the PSBP-0 sequence in order to identify a peptide with higher affinity for PS [112].

A surface-plasmon resonance (SPR) biosensory assay was used to identify 14-mer peptide PSBP-6, which displayed high affinity for PS (K_d ~100 nM) [113]. They also conjugated PSBP-6 with a single amino acid chelator (SAAC) on its *N*-terminal end, which was then labeled with ^{99m}Tc for single photon emission computed tomography (SPECT) imaging of cell death. The ability of SPECT imaging agent ^{99m}Tc-SAAC-PSBP-6 to target chemotherapy-induced tumor apoptosis was evaluated in nude mice bearing B16/F10 murine melanoma tumors, using paclitaxel chemotherapy.

In this study, biodistribution and autoradiography analyses revealed higher uptake of ^{99m}Tc-SAAC-PSBP-6 in paclitaxel-treated tumors compared to untreated tumors [113]. The same research group also conducted preclinical SPECT imaging studies in nude mice bearing B16/F10 melanoma tumors treated with paclitaxel, as well as in C3H/HeJ mice bearing 38C13 lymphoma tumors treated with cyclophosphamide. In both models of chemotherapy-induced tumor apoptosis, an increase in uptake of ^{99m}Tc-SAAC-PSBP-6 was observed in treated tumors versus untreated tumors, further demonstrating the utility of radiopeptide^{99m}Tc-SAAC-PSBP-6 for SPECT imaging of chemotherapy-induced tumor cell death [115]. With the advantages that positron emission tomography (PET) technology offers over SPECT, including higher sensitivity and

better image quality, Perreault et al. labeled the reported high affinity PS-binding peptide PSBP-6 with positron emitting radionuclide ^{64}Cu for PET imaging of cell death [116]. For this purpose, 14-mer peptide PSBP-6 was modified with an aminovaleric acid (Ava) linker and macrocyclic chelator 1,4,7-triazacyclononane-triacetic acid (NOTA). NOTA-Ava-PSBP-6 was radiolabeled with ^{64}Cu to give radiotracer ^{64}Cu-NOTA-Ava-PSBP-6. Using the same radiometric competitive binding assay against PS-bound ^{64}Cu-labeled NOTA-annexin V [109], IC_{50} values for PSBP-6, NOTA-Ava-PSBP-6 and ^{nat}Cu-NOTA-Ava-PSBP-6 were determined in the sub-millimolar range and therefore orders of magnitude lower compared to the recently studied PS-binding hexapeptides LIKKPF and PGDLSR (Fig. 6).

Conjugation of 14-mer peptide PSBP-6 with chelator NOTA via an Ava linker resulted in an increase of inhibitory potency by one order of magnitude, from 600 µM to 30 µM. Complexation of NOTA-Ava-PSBP-6 with $^{nat}Cu^{2+}$ further increased inhibitory potency as reflected by the determined IC_{50} value of 23 µM for ^{nat}Cu-NOTA-Ava-PSBP-6 [116]. However, the determined IC_{50} value of 0.6 mM for PSBP-6 reflected a significantly lower inhibitory potency for PS as previously reported by Xiong et al., who found a K_D of 0.1 µM for PSBP-6 based on surface plasmon resonance (SPR) analysis [113]. Differences may be attributed to different assays and readout values used. Also, Xiong et al. conjugated the *N*-terminus of PSBP-6 with single amino acid chelator (SAAC) lys[di(2-pyridinemethyl)]-COOH to afford SAAC-PSBP-6, which was labeled with ^{99m}Tc for SPECT imaging. SAAC-PSBP-6 showed improved binding affinity for PS over unmodified PSBP-6 presumably due to the lipophilic nature of the SAAC chelator, which strengthened interactions between the peptide and hydrophobic phospholipid. The rhenium complex of SAAC-PSBP-6 as nonradioactive surrogate for ^{99m}Tc resulted in a further increase in PS-binding affinity of the peptide (K_D 26 nM) [113]. A similar trend was observed when NOTA was attached to PSBP-6 as conjugation of 14-mer peptide PSBP-6 with NOTA chelator via an Ava linker led to a 20-fold increase of PS binding affinity [116].

Differences between SAAC-PSBP-6 and NOTA-Ava-PSBP-6 may also be attributed to different net charges of Re-SAAC-PSBP-6 and ^{64}Cu-NOTA-PSBP-6. While there is no net negative charge on ^{99m}Tc/Re-SAAC-PSBP-6, the

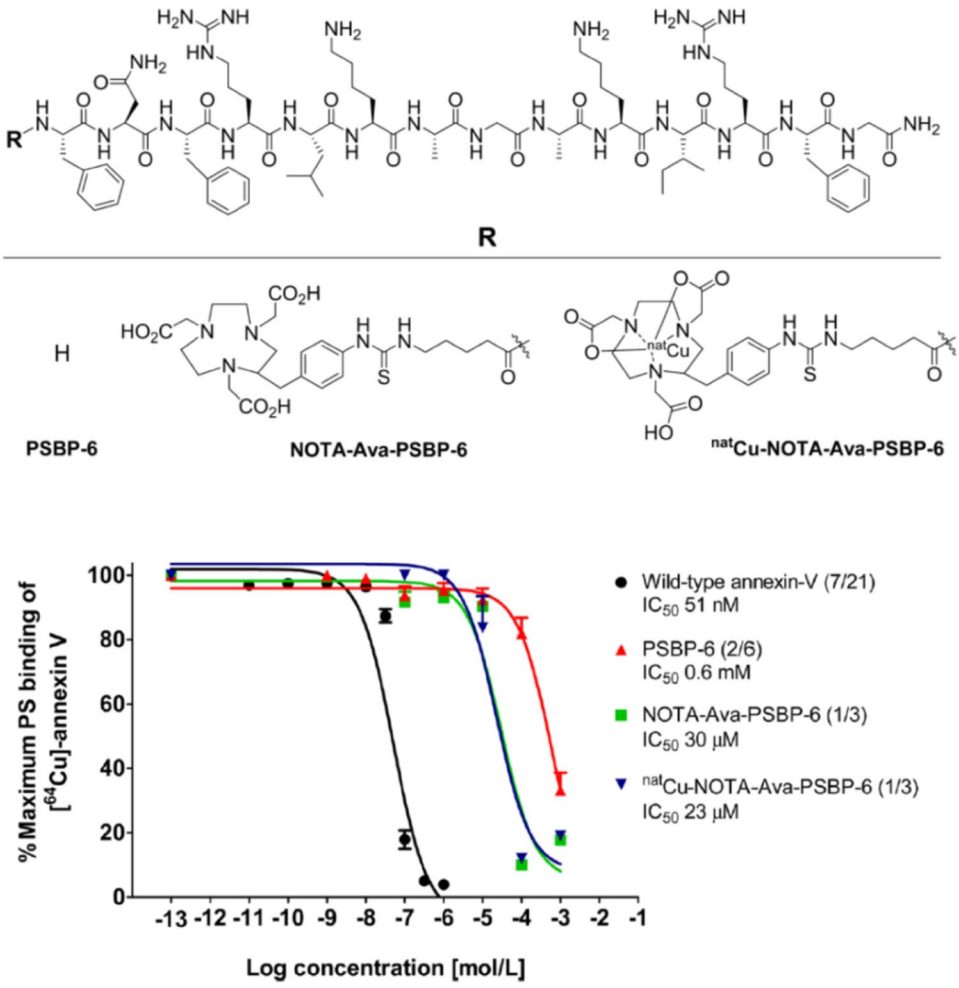

Fig. 6 Structures of PSBP-6, NOTA-Ava-PSBP-6 and ^{nat}Cu-NOTA-Ava-PSBP-6; Determination of inhibitory binding concentrations (IC_{50}) in the radiometric competition binding assay against ^{64}Cu-NOTA-annexin V. (reproduced from Perreault et al. [116])

partial coordination of bivalent $^{64}Cu^{2+}$ with two of the three carboxylate groups available for coordination on NOTA leaves one group free, producing a negative net charge. The negative charge on ^{64}Cu-NOTA-Ava-PSBP-6 might slightly interfere with binding of this radiopeptide to anionic PS due to electrostatic resistance.

However, if Ca^{2+} ions are present, these might be recruited to the negatively charged [^{64}Cu-NOTA] complex through electrostatic interactions, which would neutralize the net charge, thereby reducing electrostatic resistance and enhancing binding between ^{64}Cu-NOTA-Ava-PSBP-6 and PS. This concept would also explain the similar IC_{50} values obtained for NOTA-Ava-PSBP-6 and ^{nat}Cu-NOTA-PSBP-6, since they were determined in the presence of Ca^{2+}. Nevertheless, the ability of ^{64}Cu-NOTA-Ava-PSBP-6 to detect cell death in the absence of Ca^{2+} demonstrates a significant advantage of this PS-targeting peptide over annexin V-based probes for imaging cell death. In fact, the blood plasma of mammals normally contains only low levels of Ca^{2+}, which would favor radiopeptide ^{64}Cu-NOTA-Ava-PSBP-6 to target PS-containing cells in vivo.

Radiolabeled peptide ^{64}Cu-NOTA-Ava-PSBP-6 shows a small amount of binding to control EL4 cells, consistent with the basal level of cell death normally found in this cell line. Upon treatment with camptothecin, binding significantly increased 1.5- to twofold [116]. Xiong et al. also examined binding of SPECT agent ^{99m}Tc-SAAC-PSBP-6 to DLD1 human colon carcinoma cells treated with increasing doses of tumor necrosis factor-related apoptosis-inducing ligand (TRAIL), and found that as they increased the dose of TRAIL, binding of ^{99m}Tc-SAAC-PSBP-6 also increased [113]. Although direct comparison of these in vitro results between ^{99m}Tc-SAAC-PSBP-6 and ^{64}Cu-NOTA-Ava-PSBP-6 is difficult since the radiopeptides were analyzed using different in vitro models of cell death, both results agree that 14-mer peptide sequence FNFRLKAGAKIRFG in PSBP-6 can detect chemotherapy-induced tumor cell death.

In vivo, ^{64}Cu-NOTA-Ava-PSBP-6 showed a significantly higher (1.3-fold) uptake in treated (cocktail of cyclophosphamide (100 mg/kg) and etoposide (76 mg/kg) for 24 h) versus untreated EL4 tumors at 5 min p.i [116]. However, tumor retention of ^{64}Cu-NOTA-Ava-PSBP-6 was poor. While tumor uptake of the radiopeptide occurs quickly within 5 min, the radiopeptide is rapidly washed out and any differences between control and treated tumors is no longer visible. Song et al. have evaluated ^{99m}Tc-SAAC-PSBP-6 in vivo and found a twofold increase in tumor uptake into cyclophosphamide (100 mg/kg) treated 38C13 lymphoma tumors versus control (untreated) tumors [115]. A similar result was found in paclitaxel-treated (80 mg/kg) B16/F10 melanoma tumors. Tumor uptake of ^{99m}Tc-SAAC-PSBP-6 increased by 2.5-fold [113].

However, peptides are often rapidly degraded by endogenous peptidases in the plasma or by liver enzymes [117]. Thus, good in vivo stability is an important characteristic of peptide-based molecular imaging probes, as the radiopeptide must remain intact in the blood long enough for it to accumulate in the target tissue at sufficient concentrations. Radiopeptide ^{64}Cu-NOTA-Ava-PSBP-6 was found to be moderately stable in mice over time, with ~31% of intact radiopeptide detected after 60 min in the plasma [116]. The C-terminus of NOTA-Ava-PSBP-6 was end-capped through conversion of the carboxylic acid to an amide, which prevents metabolism by exopeptidases that target the C-terminus and thus contributes to the peptide's metabolic stability [118]. The proteolytic degradation of ^{64}Cu-NOTA-Ava-PSBP-6, as well as the binding of ^{64}Cu-NOTA-Ava-PSBP-6 to blood cells, which reduces its plasma availability for tumor uptake, both likely contribute to the washout from EL4 tumor tissue over time (Fig. 7) [116].

Despite the findings from Xiong et al. showing chemotherapy-induced increased tumor uptake of ^{99m}Tc-SAAC-PSBP-6 after 4 h p.i [113]. and Perreault et al. also analyzing chemotherapy-induced increased tumor uptake but followed by a rapid washout from tumor tissue [116], fine-tuning the peptide structure for enhanced metabolic stability and increased PS binding is necessary to generate a suitable peptide-based probe for in vivo PET imaging of apoptosis.

Cy7.5-labeled PSP-1

Linear 9-mer peptide PSP-1 (CLSYYPSYC) was also generated from a M13 phage display peptide library on PS-coated ELISA plates [119]. This peptide was initially evaluated as a FITC-labeled probe in apoptotic H460 cells in vitro and in H460 tumour-bearing mice. The peptide showed increased uptake in camptothecin-treated (10 mg/kg, 24 h prior peptide injection) H460 tumors in vivo. A more recent follow-up study used Cy7.5-labeled PSP-1 in the same animal model [120]. Binding to PS containing liposomes was analyzed by surface plasmon resonance (SPR) spectroscopy. The binding constant (K_D) was estimated to be 10.7 µM for PSP-1 in comparison to 3.15 nM for annexin V. Thus, binding of PSP-1 would be 2 orders of magnitude lower than the one determined for PSBP-6 in a similar SPR assay [113]. Analysis of Cy7.5-labeled PSP-1 (23.16 µM) and annexin V (14.3 µM) in vivo using fluorescence imaging revealed a PS-specific tumor signal for 12 h. This is indicative of a degree of irreversible peptide binding to PS keeping the optical probe effectively trapped. Further studies are required to better understand this phenomenon.

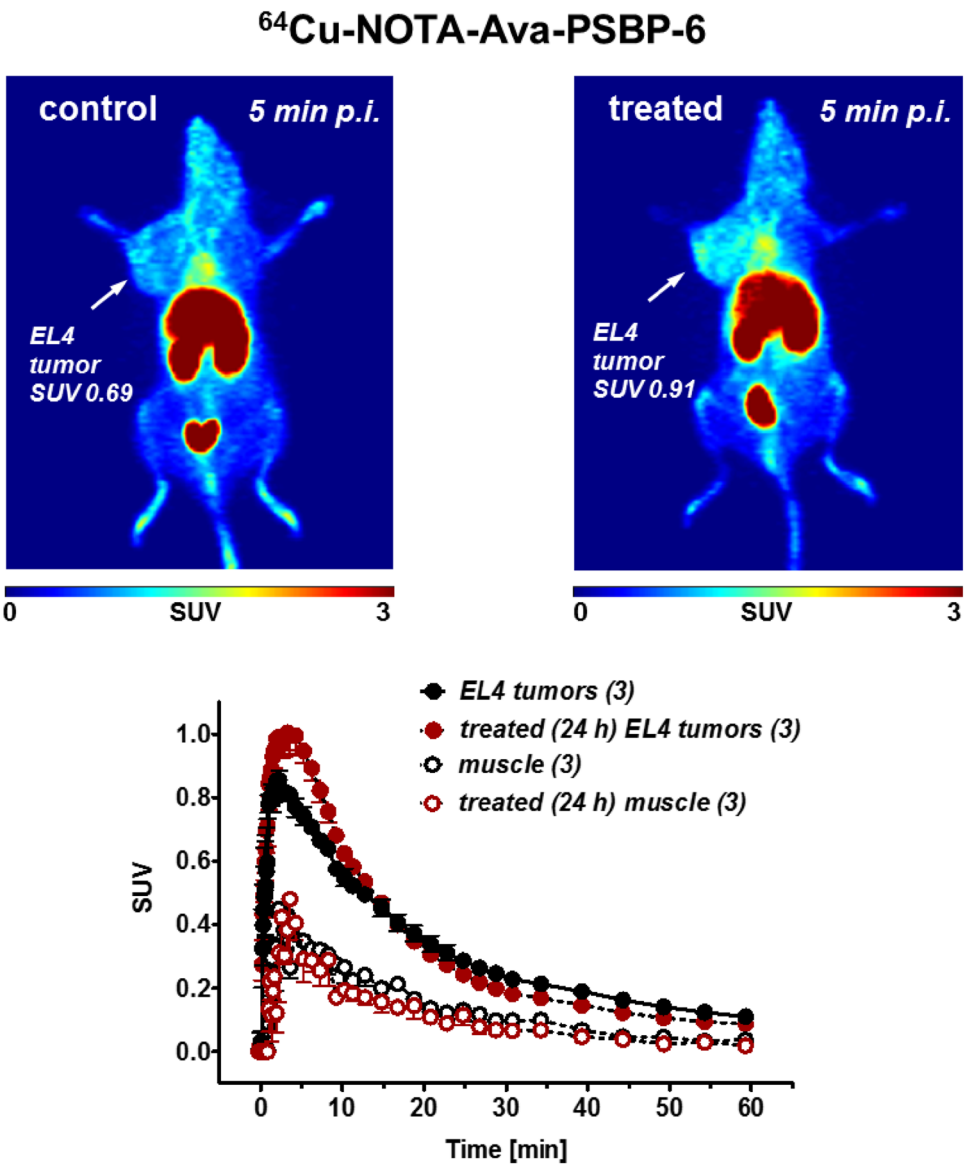

Fig. 7 PET images as maximum-intensity projections of EL4 tumor bearing C57Bl6 mice in response to treatment with cyclophosphamide and etoposide after injection of ^{64}Cu-NOTA-Ava-PSBP-6 (reproduced from Perreault et al. [116])

Peptide-peptoid hybrid PPS1D1

Starting from monomeric peptide PPS1, Udugamasooriya and co-workers evaluated a mini-library of dimeric peptid-peptoid hybrid structures of PPS1D1 to define a mini pharmacophore essential for optimal binding to lipid-PS [121, 122]. As a result, it was found that dimerization at the C-terminal leads to increased cytotoxicity. Binding of the FITC-labeled lead structure peptide PPS1D1 to immobilized PS in an ELISA-like binding assay was completely inhibited at a 1 µM concentration of PPS1D1 [122]. This study found that the distinct positive charge and all four hydrophobic residues at the N-terminus are essential for the interaction with the hydrophobic tail region of the PS phospholipid. It was found that switching the linker from the C-terminus to an internal position, increasing hydrophobic regions at the N-terminus, and increasing the number of positive charges to four keeps the binding potency towards PS in a similar range to lead structure PPS1D1 [123]. It remains to be elucidated if this very carefully generated peptide structure would be a suitable peptide for molecular imaging of apoptosis in vivo.

Cyclic peptides mimicking lactadherin and binding to PS

An alternative approach has been introduced by Zheng et al. [124]. who have developed lactadherin-mimicking cyclic peptide structures (cLACs) which bind to PS at low micromolar affinities. Optimization of oligoglycine linkers were following the lipid binding mode of lactadherin.

Attaching a fluorescein label to a selected cLAC-2 structure revealed selective binding to PS in camptothecin-treated

Jurkat cells [124]. A follow-up study improved the synthesis of these cyclic peptides by using native chemical ligation chemistry [125]. This approach takes advantage of the orthogonal reactivity of an N-terminal cysteine and a C-terminal thioester and represents a more general synthesis method for efficient preparation of cyclic peptides which was used to generate the lactadherin-mimicking PS binding peptides [124]. However, no radiolabeling with reported cyclic peptides for PET or SPECT imaging has been reported.

^{124}I-labeled antibody fragment PGN635 F(ab'2)

In addition to a variety of PS-binding PET and SPECT agents based on peptides, one radiolabeled antibody fragment has also been investigated for this application [126]. F(ab'2) fragments from the human PS-targeting antibody PGN635 were generated by incubating the antibody with pepsin. The resulting purified F(ab'2) fragments were radiolabeled with ^{124}I or ^{125}I with a labeling efficiency of 14 to 19%. The choice of radioisotope did not change the binding affinity of the PGN635 F(ab'2) fragment towards PS as determined in a competition ELISA assay. In vivo stability was determined in mice and no evidence was found of lower molecular weight ^{124}I-labeled degradation products or free ^{124}I. In vivo analysis in mice revealed uptake in PC-3 tumours of 1.2% ID/g at 48 h p.i [126].

Treatment with the chemotherapy agent docetaxel as well as radiation therapy with 15 Gy increased PC3 tumor uptake of ^{124}I-PGN635 F(ab'2). However, detailed assessment of PS after both treatment protocols of these PC3 tumors was missing. Despite the potential suitability of the PGN635 F(ab'2) fragment for PET imaging of early apoptosis, use of ^{124}I with its long half-life (4.18 days) and reaching the most optimal tumor-to-background ratio only after 48 h, means that this approach may not be favorable for clinical translation. Further developments from the same research group have led toa PGN635 antibody-decorated superparamagnetic iron oxide nanoparticle as an MRI/optical dual-modality imaging probe and antibody-decorated liposomes for drug delivery [127]. They showed excellent tumor contrast in MDA-MB231 breast cancer models.

Phosphatidylserine-binding Zn(II) complexes

Insights into the binding mechanism of annexin V to the phosphoserine head group of PS via Ca^{2+} raised the possibility to design coordination compounds containing Zn^{2+} cations as phosphate chemosensors and functional mimics of annexin V. The concept of detecting PS in apoptotic cells using low-molecular weight Zn^{2+} coordination compounds was first demonstrated with compound PSS-380 [128]. Fluorescence-sensing compound PSS-380 is an anthracene derivative containing two Zn^{2+} dipicolamine groups. Numerous Zn^{2+} dipicolylamine complexes have been reported for recognition and sensing PS in dying cells mainly based on their fluorescence properties [129].

The ability to detect PS in dying cells with Zn^{2+}-bis(dipicolylamine) (Zn-BDPA) coordination complexes is driven by a combination of electrostatic attraction to the anionic membrane and Zn^{2+} ion coordination by the phosphate and carboxylate motifs of the PS headgroup (Fig. 8) [130].

The use of radiolabeled small molecule Zn^{2+} complexes for imaging of PS in apoptotic cells was first reported with ^{18}F-labeled Zn^{2+}-bis(cyclen) complexes [131]. Increased uptake of PS targeting Zn^{2+} complex $[Zn_2(^{18}F\text{-}6]^{4+}$ was demonstrated with PET imaging of HeLaMatu tumors after taxol treatment. More recently, a ^{11}C-labeled bis-Zn^{2+}-cyclen complex was used for PET imaging of apoptosis in S-180 fibrosarcomas in mice upon treatment with cyclophosphamide [132].

Several publications also describe radiolabeled Zn^{2+}-dipicolyalamine complexes for SPECT and PET imaging of apoptosis in vivo using ^{99m}Tc and ^{18}F as radionuclides, respectively [133–136]. Interestingly, compound [18F]FP-DPAZn_2 was proposed as potential small-molecule radiotracer for PET imaging of cell death in Alzheimer's disease [136]. Structures of selected radiolabeled low molecular weight Zn^{2+} complexes for PS imaging is given in Fig. 9.

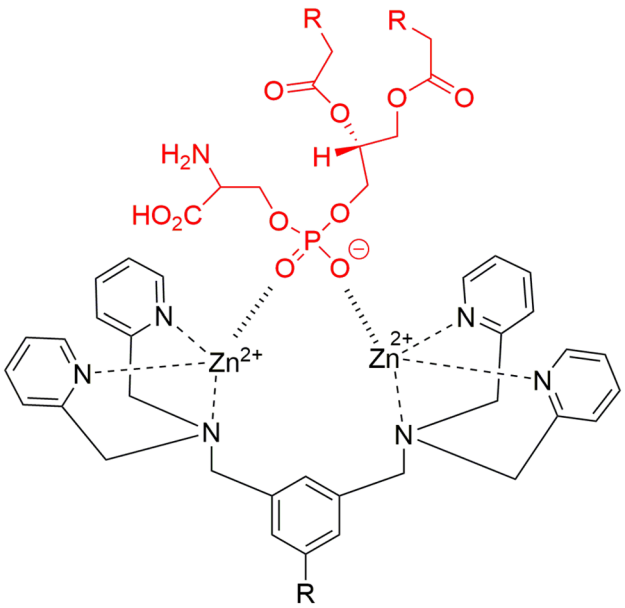

Fig. 8 Proposed binding mode of Zn^{2+}-bis(dipicolylamine) complexes to PS (red) *(adapted from Plaunt* et al. [130]*)*

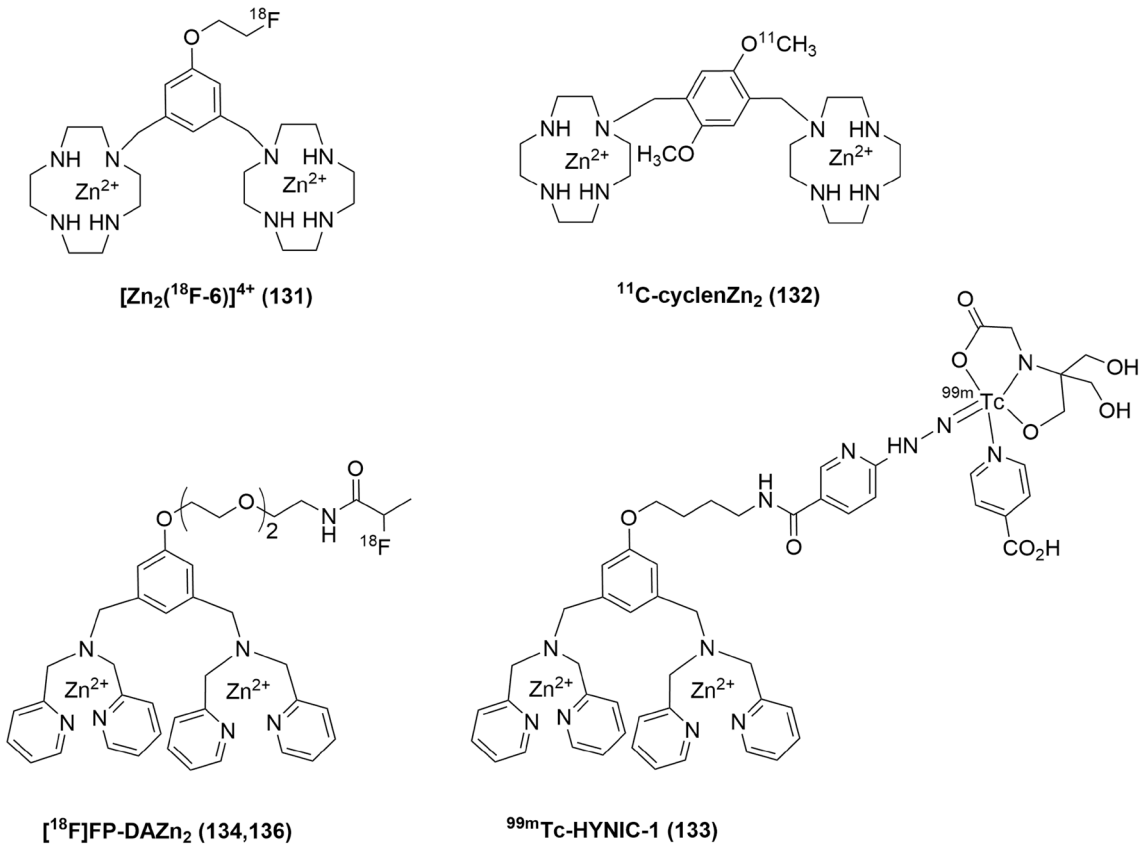

Fig. 9 Selection of radiolabeled Zn^{2+} complexes (top: Zn^{2+}-bis-cyclens; bottom: Zn^{2+} bis-dipicolylamines as PS imaging agents

Conclusion

As derived from numerous clinical trials, ^{99m}Tc-annexin V still represents the radiotracer of choice for imaging apoptosis through targeting PS [137]. However, with radiolabeled annexin V a number of drawbacks are apparent, including: (i) complex and expensive radiolabeling procedures, (ii) poor biodistribution profiles displaying high nonspecific uptake in liver and kidneys, (iii) slow blood clearance resulting in poor image contrast, (iv) inability to control Ca^{2+} concentrations in vivo, (v) poor tumor tissue penetration, and (vi) lack of knowledge of the optimal imaging time after cell death has been induced and radiolabeled annexin V has been administered. Therefore, alternative strategies and concepts for the development of PS-binding radiotracers are needed. Peptides represent an alternative and promising strategy to target PS. They provide several advantages over annexin V including better pharmacokinetics due to their smaller size, better availability, and simpler synthesis and radiolabeling strategies. So far, most of the generated peptide derivatives have been identified through phage-display or combinatorial screening approaches. While binding to PS was validated in vitro and peptides such as PSBP-6 have been found to bind in the medium-to-low micromolar range, lack of metabolic stability in vivo still represents a major challenge for their application as molecular imaging probes. Therefore, there is still a need to optimize selected peptide structures for potential translational use as imaging agents for apoptosis through targeting PS.

In addition to radiolabeled peptides, various ^{11}C, ^{18}F and ^{99m}Tc-labeled low-molecular weight Zn^{2+} complexes have been described as targeting vectors for PS in apoptotic cells. This interesting class of compounds particularly holds great promise for future clinical translation to monitor cell death in patients with neurodegenerative diseases like Alzheimer's disease through their ability to cross the blood–brain barrier.

Acknowledgements We gratefully acknowledge the support of this research by the Dianne and Irving Kipnes Foundation, the Alberta Cancer Foundation (ACF) and the Canadian Foundation for Innovation (CFI).

Compliance with ethical standards

Conflict of interest The authors declare no conflict of interest.

References

1. Kerr JF, Wylie AH, Currie AR (1972) Apoptosis: the basic biological phenomenon with wide-ranging implications in tissue kinetics. Br J Cancer 26:239–257
2. Fulda S, Debatin KM (2006) Extrinsic versus intrinsic apoptosis pathways in anticancer chemotherapy. Oncogene 25:4798–4811
3. Hengartner MO (2000) The biochemistry of apoptosis. Nature 407:770–777
4. Syeed SA, Vohra H, Gupta A, Ganguly NK (2001) Apoptosis: molecular machinery. Curr Sci 80:349–360
5. Martin SJ, Reutelingsperger CP, McGahon AJ, Rader JA, van Schie RC, La Face DM, Green DR (1995) Early redistribution of plasma membrane phosphatidylserine is a general feature of apoptosis regardless of the initiating stimulus: inhibition by overexpression of Bcl-2 and Abl. J Exp Med 182:1545–1556
6. Schutters K, Reutelingsperger C (2010) Phosphatidylserine targeting for diagnosis and treatment of human diseases. Apoptosis 15:1072–1082
7. Zwaal RF, Comfurius P, Bevers EM (2005) Surface exposure of phosphatidylserine in pathological cells. Cell Mol Life Sci 62:971–988
8. Saikumar P, Dong Z, Mikhailov V, Denton M, Weinberg JM, Venkatachalam MA (1999) Apoptosis: definition, mechanisms, and relevance to disease. Am J Med 107:489–506
9. Green AM, Steinmetz ND (2002) Monitoring apoptosis in real time. Cancer J 8:82–92
10. Boersma HH, Kietselaer BL, Stolk LM, Bennaghmouch A, Hofstra L, Narula J, Heidendal GA, Reutelingsperger CP (2005) Past, present, and future of annexin A5: from protein discovery to clinical applications. J Nucl Med 46:2035–2050
11. Gerke V, Moss SE (2002) Annexins: from structure to function. Physiol Rev 82:331–371
12. Lahorte CM, Vanderheyden JL, Steinmetz N, Van de Wiele C, Dierckx RA, Slegers G (2004) Apoptosis-detecting radioligands: current state of the art and future perspectives. Eur J Nucl Med 31:887–910
13. Bazzi MD, Nelsestuen GL (1991) Highly sequential binding of protein kinase C and related proteins to membranes. Biochemistry 30:7970–7977
14. Koopman G, Reutelingsperger CP, Kuijten GA, Keehnen RM, Pals ST, van Oers MH (1994) Annexin V for flow cytometric detection of phosphatidylserine expression on B cells undergoing apoptosis. Blood 84:1415–1420
15. Thiagarajan P, Tait JF (1990) Binding of annexin V/placental anticoagulant protein I to platelets. Evidence for phosphatidylserine exposure in the procoagulant response of activated platelets. J Biol Chem 265:17420–17423
16. Lahorte C, Dumont F, Slegers G, Van De Wiele C, Dierckx RA, Philippe J (2000) Synthesis and in vitro stability of 123I-labelled annexin V: a potential agent for spect imaging of apoptotic cells. J Labelled Cpd Radiopharm 43:739–751
17. Lahorte C, Slegers G, Philippé J, Van de Wiele C, Dierckx RA (2001) Synthesis and in vitro evaluation of 123I-labelled human recombinant annexin V. Biomol Eng 17:51–53
18. Rao LV, Tait JF, Hoang AD (1992) Binding of annexin V to a human ovarian carcinoma cell line (OC-2008). Contrasting effects on cell surface factor VIIa/tissue factor activity and prothrombinase activity. Thromb Res 67:517–531
19. Lahorte CM, van de Wiele C, Bacher K, van den Bossche B, Thierens H, van Belle S, Slegers G, Dierckx RA (2003) Biodistribution and dosimetry study of 123I-rh-annexin V in mice and humans. Nucl Med Commun 24:871–880
20. Russell J, O'Donoghue JA, Finn R, Koziorowski J, Ruan S, Humm JL, Ling CC (2002) Iodination of annexin V for imaging apoptosis. J Nucl Med 43:671–677
21. Eisenhut M (2006) Molecular position of radiolabels and its impact on functional integrity of proteins. J Nucl Med 47:1400–1402
22. Stratton JR, Dewhurst TA, Kasina S, Reno JM, Cerqueira MD, Baskin DG, Tait JF (1995) Selective uptake of radiolabeled annexin V on acute porcine left atrial thrombi. Circulation 92:3113–3121
23. Tait JF, Cerqueira MD, Dewhurst TA, Fujikawa K, Ritchie JL, Stratton JR (1994) Evaluation of annexin V as a platelet-directed thrombus targeting agent. Thromb Res 75:491–501
24. Kown MH, Strauss HW, Blankenberg FG, Berry GJ, Stafford-Cecil S, Tait JF, Goris ML, Robbins RC (2001) In vivo imaging of acute cardiac rejection in human patients using (99 m) technetium labeled annexin V. Am J Transplant 1:270–277
25. Narula J, Acio ER, Narula N, Samuels LE, Fyfe B, Wood D, Fitzpatrick JM, Raghunath PN, Tomaszewski JE, Kelly C, Steinmetz N, Green A, Tait JF, Leppo J, Blankenberg FG, Jain D, Strauss HW (2001) Annexin-V imaging for noninvasive detection of cardiac allograft rejection. Nat Med 7:1347–1352
26. Belhocine T, Steinmetz N, Hustinx R, Bartsch P, Jerusalem G, Seidel L, Rigo P, Green A (2002) Increased uptake of the apoptosis-imaging agent (99 m)Tc recombinant human Annexin V in human tumors after one course of chemotherapy as a predictor of tumor response and patient prognosis. Clin Cancer Res 8:2766–2774
27. Kemerink GJ, Boersma HH, Thimister PW, Hofstra L, Liem IH, Pakbiers MT, Janssen D, Reutelingsperger CP, Heidendal GA (2001) Biodistribution and dosimetry of 99mTc-BTAP-annexin-V in humans. Eur J Nucl Med 28:1373–1378
28. Boersma HH, Liem IH, Kemerink GJ, Thimister PW, Hofstra L, Stolk LM, van Heerde WL, Pakbiers MT, Janssen D, Beysens AJ, Reutelingsperger CP, Heidendal GA (2003) Comparison between human pharmacokinetics and imaging properties of two conjugation methods for 99mTc-annexin A5. Br J Radiol 76:553–560
29. Blankenberg FG, Katsikis PD, Tait JF, Davis RE, Naumovski L, Ohtsuki K, Kopiwoda S, Abrams MJ, Darkes M, Robbins RC, Maecker HT, Strauss HW (1998) In vivo detection and imaging of phosphatidylserine expression during programmed cell death. Proc Natl Acad Sci USA 95:6349–6354
30. Blankenberg FG, Katsikis PD, Tait JF, Davis RE, Naumovski L, Ohtsuki K, Kopiwoda S, Abrams MJ, Strauss HW (1999) Imaging of apoptosis (programmed cell death) with 99mTc annexin V. J Nucl Med 40:184–191
31. Vriens PW, Blankenberg FG, Stoot JH, Ohtsuki K, Berry GJ, Tait JF, Strauss HW, Robbins RC (1998) The use of technetium Tc 99 m annexin V for in vivo imaging of apoptosis during cardiac allograft rejection. J Thorac Cardiovasc Surg 116:844–853
32. Ohtsuki K, Akashi K, Aoka Y, Blankenberg FG, Kopiwoda S, Tait JF, Strauss HW (1999) Technetium-99m HYNIC-annexin V: a potential radiopharmaceutical for the in-vivo detection of apoptosis. Eur J Nucl Med 26:1251–1258
33. Blankenberg FG, Robbins RC, Stoot JH, Vriens PW, Berry GJ, Tait JF, Strauss HW (2000) Radionuclide imaging of acute lung transplant rejection with annexin V. Chest 117:834–840
34. Ogura Y, Krams SM, Martinez OM, Kopiwoda S, Higgins JP, Esquivel CO, Strauss HW, Tait JF, Blankenberg FG (2000) Radiolabeled annexin V imaging: diagnosis of allograft rejection in an experimental rodent model of liver transplantation. Radiology 214:795–800
35. Blankenberg FG, Tait JF, Blankenberg TA, Post AM, Strauss HW (2001) Imaging macrophages and the apoptosis of granulocytes in a rodent model of subacute and chronic abscesses with

radiolabeled monocyte chemotactic peptide-1 and annexin V. Eur J Nucl Med 28:1384–1393
36. Blankenberg FG, Naumovski L, Tait JF, Post AM, Strauss HW (2001) Imaging cyclophosphamide-induced intramedullary apoptosis in rats using 99mTc-radiolabeled annexin V. J Nucl Med 42:309–316
37. Tokita N, Hasegawa S, Maruyama K, Izumi T, Blankenberg FG, Tait JF, Strauss HW, Nishimura T (2003) 99mTc-Hynic-annexin V imaging to evaluate inflammation and apoptosis in rats with autoimmune myocarditis. Eur J Nucl Med Mol Imaging 30:232–238
38. Post AM, Katsikis PD, Tait JF, Geaghan SM, Strauss HW, Blankenberg FG (2002) Imaging cell death with radiolabeled annexin V in an experimental model of rheumatoid arthritis. J Nucl Med 43:1359–1365
39. Taki J, Higuchi T, Kawashima A, Tait JF, Kinuya S, Muramori A, Matsunari I, Nakajima K, Tonami N, Strauss HW (2004) Detection of cardiomyocyte death in a rat model of ischemia and reperfusion using 99mTc-labeled annexin V. J Nucl Med 45:1536–1541
40. Peker C, Sarda-Mantel L, Loiseau P, Rouzet F, Nazneen L, Martet G, Vrigneaud JM, Meulemans A, Saumon G, Michel JB, Le Guludec D (2004) Imaging apoptosis with (99 m)Tc-annexin-V in experimental subacute myocarditis. J Nucl Med 45:1081–1086
41. Tang XN, Wang Q, Koike MA, Cheng D, Goris ML, Blankenberg FG, Yenari MA (2007) Monitoring the protective effects of minocycline treatment with radiolabeled annexin V in an experimental model of focal cerebral ischemia. J Nucl Med 48:1822–1828
42. Mochizuki T, Kuge Y, Zhao S, Tsukamoto E, Hosokawa M, Strauss HW, Blankenberg FG, Tait JF, Tamaki N (2003) Detection of apoptotic tumor response in vivo after a single dose of chemotherapy with 99mTc-annexin V. J Nucl Med 44:92–97
43. Wong E, Kumar V, Howman-Giles RB, Vanderheyden JL (2008) Imaging of therapy-induced apoptosis using (99 m)Tc-HYNIC-annexin V in thymoma tumor-bearing mice. Cancer Biother Radiopharm 23:715–726
44. Lan XL, Zhang YX, He Y, Sun X, An R, Gao ZR, Cao GX (2008) Feasibility of apoptosis-imaging agent 99mTc-HYNIC-annexin V in early assessment of chemotherapeutic effect on tumor models. Zhonghua Zhong Liu Za Zhi 30:737–740
45. Guo MF, Zhao Y, Tian R, Li L, Guo L, Xu F, Liu YM, He YB, Bai S, Wang J (2009) In vivo 99mTc-HYNIC-annexin V imaging of early tumor apoptosis in mice after single dose irradiation. J Exp Clin Cancer Res. 28:136
46. Erba PA, Manfredi C, Lazzeri E, Minichilli F, Pauwels EK, Sbrana A, Strauss HW, Mariani G (2010) Time course of Paclitaxel-induced apoptosis in an experimental model of virus-induced breast cancer. J Nucl Med 51:775–781
47. Kemerink GJ, Liu X, Kieffer D, Ceyssens S, Mortelmans L, Verbruggen AM, Steinmetz ND, Vanderheyden JL, Green AM, Verbeke K (2003) Safety, biodistribution, and dosimetry of 99mTc-HYNIC-annexin V, a novel human recombinant annexin V for human application. J Nucl Med 44:947–952
48. Thimister PW, Hofstra L, Liem IH, Boersma HH, Kemerink G, Reutelingsperger CP, Heidendal GA (2003) In vivo detection of cell death in the area at risk in acute myocardial infarction. J Nucl Med 44:391–396
49. Kiestelaer BLJH, Reutelingsperger CPM, Heidendal GAK, Daemen MJAP, Mess WH, Hofstra L (2004) Noninvasive detection of plaque instability with use of radiolabeled annexin A5 in patients with carotid-artery atherosclerosis. N Engl J Med 350:1472–1473
50. Blankenberg FG, Kalinyak J, Liu L, Koike M, Cheng D, Goris ML, Green A, Vanderheyden JL, Tong DC, Yenari MA (2006) 99mTc-HYNIC-annexin V SPECT imaging of acute stroke and its response to neuroprotective therapy with antiFas ligand antibody. Eur J Nucl Med Mol Imaging 33:566–574
51. Lorberboym M, Blankenberg FG, Sadeh M, Lampl Y (2006) In vivo imaging of apoptosis in patients with acute stroke: correlation with blood-brain barrier permeability. Brain Res 1103:13–19
52. Lampl Y, Lorberboym M, Blankenberg FG, Sadeh M, Gilad R (2006) Annexin V SPECT imaging of phosphatidylserine expression in patients with dementia. Neurology 66:1253–1254
53. van de Wiele C, Lahorte C, Vermeersch H, Loose D, Mervillie K, Steinmetz ND, Vanderheyden JL, Cuvelier CA, Slegers G, Dierck RA (2003) Quantitative tumor apoptosis imaging using technetium-99m-HYNIC annexin V single photon emission computed tomography. J Clin Oncol 21:3483–3487
54. Vermeersch H, Loose D, Lahorte C, Mervillie K, Dierckx R, Steinmetz N, Vanderheyden JL, Cuvelier C, Slegers G, Van de Wiele C (2004) 99mTc-HYNIC Annexin-V imaging of primary head and neck carcinoma. Nucl Med Commun 25:259–263
55. Rongen GA, Oyen WJ, Ramakers BP, Riksen NP, Boerman OC, Steinmetz N, Smits P (2005) Annexin A5 scintigraphy of forearm as a novel in vivo model of skeletal muscle preconditioning in humans. Circulation 111:173–178
56. Riksen NP, Oyen WJ, Ramakers BP, Van den Broek PH, Engbersen R, Boerman OC, Smits P, Rongen GA (2005) Oral therapy with dipyridamole limits ischemia-reperfusion injury in humans. Clin Pharmacol Ther 78:52–59
57. Riksen NP, Zhou Z, Oyen WJ, Jaspers R, Ramakers BP, Brouwer RM, Boerman OC, Steinmetz N, Smits P, Rongen GA (2006) Caffeine prevents protection in two human models of ischemic preconditioning. J Am Coll Cardiol 48:700–707
58. Haas RL, de Jong D, Olmos RAV, Hoefnagel CA, van den Heuvel I, Zerp SF, Bartelink H (2004) Verheij, M. In vivo imaging of radiation induced apoptosis in follicular lymphoma patients. Int J Radiat Oncol Biol Phys 59:782–787
59. Kartachova M, Haas RL, Olmos RA, Hoebers FJ, van Zandwijk N, Verheij M (2004) In vivo imaging of apoptosis by 99mTc-Annexin V scintigraphy: visual analysis in relation to treatment response. Radiother Oncol 72:333–339
60. Rottey S, Slegers G, Van Belle S, Goethals I, Van de Wiele C (2006) Sequential 99mTc-hydrazinonicotinamide-annexin V imaging for predicting response to chemotherapy. J Nucl Med 47:1813–1818
61. Rottey S, Loose D, Vakaet L, Lahorte C, Vermeersch H, Van Belle S, Van de Wiele C (2007) 99mTc-HYNIC Annexin-V imaging of tumors and its relationship to response to radiotherapy and/or chemotherapy. Q J Nucl Med Mol Imaging 51:182–188
62. Hoebers FJ, Kartachova M, de Bois J, van den Brekel MW, van Tinteren H, van Herk M, Rasch CR, Valdés Olmos RA, Verheij M (2008) 99mTc Hynic-rh-Annexin V scintigraphy for in vivo imaging of apoptosis in patients with head and neck cancer treated with chemoradiotherapy. Eur J Nucl Med Mol Imaging 35:509–518
63. Decristoforo C, Mather SJ (1999) Technetium-99m somatostatin analogues: effect of labelling methods and peptide sequence. Eur J Nucl Med 26:869–876
64. Verbeke K, Kieffer D, Vanderheyden JL, Reutelingsperger C, Steinmetz N, Green A, Verbruggen A (2003) Optimization of the preparation of 99mTc-labeled Hynic-derivatized Annexin V for human use. Nucl Med Biol 30:771–778
65. Vanderheyden JL, Liu G, He J, Patel B, Tait JF, Hnatowich DJ (2006) Evaluation of 99mTc-MAG3-annexin V: influence of the chelate on in vitro and in vivo properties in mice. Nucl Med Biol 33:135–144
66. Yang DJ, Azhdarinia A, Wu P, Yu DF, Tansey W, Kalimi SK, Kim EE, Podoloff DA (2001) In vivo and in vitro measurement

of apoptosis in breast cancer cells using 99mTc-EC-annexin V. Cancer Biother Radiopharm 16:73–83
67. Blankenberg F (2002) To scan or not to scan, it is a question of timing: technetium-99m-annexin V radionuclide imaging assessment of treatment efficacy after one course of chemotherapy. Clin Cancer Res 8:2757–2758
68. Kurihara H, Yang DJ, Cristofanilli M, Erwin WD, Yu DF, Kohanim S, Mendez R, Kim EE (2008) Imaging and dosimetry of 99mTc EC annexin V: preliminary clinical study targeting apoptosis in breast tumors. Appl Radiat Isot 66:1175–1182
69. Tait JF, Brown DS, Gibson DF, Blankenberg FG, Strauss HW (2000) Development and characterization of annexin V mutants with endogenous chelation sites for (99 m)Tc. Bioconjug Chem 11:918–925
70. Tait JF, Smith C, Levashova Z, Patel B, Blankenberg FG, Vanderheyden JL (2006) Improved detection of cell death in vivo with annexin V radiolabeled by site-specific methods. J Nucl Med 47:1546–1553
71. Tait JF, Smith C, Blankenberg FG (2005) Structural requirements for in vivo detection of cell death with 99mTc-annexin V. J Nucl Med 46:807–815
72. Luo QY, Wang F, Zhang ZY, Zhang Y, Lu HK, Sun SH, Zhu RS (2008) Preparation and bioevaluation of (99 m)Tc-HYNIC-annexin B1 as a novel radioligand for apoptosis imaging. Apoptosis 13:600–608
73. Fonge H, de Saint Hubert M, Vunckx K, Rattat D, Nuyts J, Bormans G, Ni Y, Reutelingsperger C, Verbruggen A (2008) Preliminary in vivo evaluation of a novel 99mTc-labeled HYNIC-cys-annexin A5 as an apoptosis imaging agent. Bioorg Med Chem Lett 18:3794–3798
74. Greupink R, Sio CF, Ederveen A, Orsel J (2009) Evaluation of a 99mTc-labeled AnnexinA5 variant for non-invasive SPECT imaging of cell death in liver, spleen and prostate. Pharm Res 26:2647–2656
75. Biechlin ML, Bonmartin A, Gilly FN, Fraysse M, du Moulinet d'Hardemare A (2008) Radiolabeling of annexin A5 with (99 m) Tc: comparison of HYNIC-Tc vs. iminothiolane-Tc-tricarbonyl conjugates. Nucl Med Biol 35:679–687
76. Vangestel C, Peeters M, Oltenfreiter R, D'Asseler Y, Staelens S, Van Steenkiste M, Philippé J, Kusters D, Reutelingsperger C, Van Damme N, Van de Wiele C (2010) In vitro and in vivo evaluation of [99mTc]-labeled tricarbonyl His-annexin A5 as an imaging agent for the detection of phosphatidylserine-expressing cells. Nucl Med Biol 37:965–975
77. De Saint-Hubert M, Mottaghy FM, Vunckx K, Nuyts J, Fonge H, Prinsen K, Stroobants S, Mortelmans L, Deckers N, Hofstra L, Reutelingsperger CP, Verbruggen A, Rattat D (2010) Site-specific labeling of 'second generation' annexin V with 99mTc(CO)3 for improved imaging of apoptosis in vivo. Bioorg Med Chem 18:1356–1363
78. Wen X, Wu QP, Ke S, Wallace S, Charnsangavej C, Huang P, Liang D, Chow D, Li C (2003) Improved radiolabeling of PEGylated protein: PEGylated annexin V for noninvasive imaging of tumor apoptosis. Cancer Biother Radiopharm 18:819–827
79. Glaser M, Collingridge DR, Aboagye EO, Bouchier-Hayes L, Hutchinson OC, Martin SJ, Price P, Brady F, Luthra SK (2003) Iodine-124 labelled annexin-V as a potential radiotracer to study apoptosis using positron emission tomography. Appl Radiat Isot 58:55–62
80. Collingridge DR, Glaser M, Osman S, Barthel H, Hutchinson OC, Luthra SK, Brady F, Bouchier-Hayes L, Martin SJ, Workman P, Price P, Aboagye EO (2003) In vitro selectivity, in vivo biodistribution and tumour uptake of annexin V radiolabelled with a positron emitting radioisotope. Br J Cancer 89:1327–1333
81. Dekker B, Keen H, Shaw D, Disley L, Hastings D, Hadfield J, Reader A, Allan D, Julyan P, Watson A, Zweit J (2005) Functional comparison of annexin V analogues labeled indirectly and directly with iodine-124. Nucl Med Biol 32:403–413
82. Keen HG, Dekker BA, Disley L, Hastings D, Lyons S, Reader AJ, Ottewell P, Watson A, Zweit J (2005) Imaging apoptosis in vivo using 124I-annexin V and PET. Nucl Med Biol 32:395–402
83. Dekker B, Keen H, Lyons S, Disley L, Hastings D, Reader A, Ottewell P, Watson A, Zweit (2005) J. MBP-annexin V radiolabeled directly with iodine-124 can be used to image apoptosis in vivo using PET. Nucl Med Biol 32:241–252
84. Zijlstra S, Gunawan J, Burchert W (2003) Synthesis and evaluation of a 18F-labelled recombinant annexin-V derivative, for identification and quantification of apoptotic cells with PET. Appl Radiat Isot 58:201–207
85. Toretsky J, Levenson A, Weinberg IN, Tait JF, Uren A, Mease RC (2004) Preparation of F-18 labeled annexin V: a potential PET radiopharmaceutical for imaging cell death. Nucl Med Biol 31:747–752
86. Grierson JR, Yagle KJ, Eary JF, Tait JF, Gibson DF, Lewellen B, Link JM, Krohn KA (2004) Production of [F-18]fluoroannexin for imaging apoptosis with PET. Bioconjug Chem 15:373–379
87. Murakami Y, Takamatsu H, Taki J, Tatsumi M, Noda A, Ichise R, Tait JF, Nishimura S (2004) 18F-labelled annexin V: a PET tracer for apoptosis imaging. Eur J Nucl Med Mol Imaging 31:469–474
88. Yagle KJ, Eary JF, Tait JF, Grierson JR, Link JM, Lewellen B, Gibson DF, Krohn KA (2005) Evaluation of 18F-annexin V as a PET imaging agent in an animal model of apoptosis. J Nucl Med 46:658–666
89. Hu S, Kiesewetter DO, Zhu L, Guo N, Gao H, Liu G, Hida N, Lang L, Niu G, Chen X (2012) Longitudinal PET imaging of doxorubicin-induced cell death with 18F-Annexin V. Mol Imaging Biol 14:762–770
90. Perreault A, Knight JC, Wang M, Way J, Wuest F (2016) 18F-Labeled wild-type annexin V: comparison of random and site-selective radiolabeling methods. Amino Acids 48:65–74
91. Li X, Link JM, Stekhova S, Yagle KJ, Smith C, Krohn KA, Tait JF (2008) Site-specific labeling of annexin V with F-18 for apoptosis imaging. Bioconjug Chem 19:1684–1688
92. Wuest F, Berndt M, Bergmann R, van den Hoff J, Pietzsch J (2008) Synthesis and application of [18F]FDG-maleimidehexyloxime ([18F]FDG-MHO): a [18F]FDG-based prosthetic group for the chemoselective 18F-labeling of peptides and proteins. Bioconjug Chem 19:1202–1210
93. Wang MW, Wang F, Zheng YJ, Zhang YJ, Zhang YP, Zhao Q, Shen CK, Wang Y, Sun SH (2013) An in vivo molecular imaging probe (18)F-Annexin B1 for apoptosis detection by PET/CT: preparation and preliminary evaluation. Apoptosis 18:238–247
94. Cauchon N, Langlois R, Rousseau JA, Tessier G, Cadorette J, Lecomte R, Hunting DJ, Pavan RA, Zeisler SK, van Lier JE (2007) PET imaging of apoptosis with (64)Cu-labeled streptavidin following pretargeting of phosphatidylserine with biotinylated annexin-V. Eur J Nucl Med Mol Imaging 34:247–258
95. Bauwens M, De Saint-Hubert M, Devos E, Deckers N, Reutelingsperger C, Mortelmans L, Himmelreich U, Mottaghy FM, Verbruggen A (2011) Site-specific 68 Ga-labeled Annexin A5 as a PET imaging agent for apoptosis. Nucl Med Biol 38:381–392
96. Davletov BA, Sudhof TC (1993) A single C2 domain from synaptotagmin I is sufficient for high affinity Ca2+/ phospholipid binding. J Biol Chem 268:26386–26390
97. Zhao M, Zhu X, Ji S, Zhou J, Ozker KS, Fang W, Molthen RC, Hellman RS (2006) 99mTc-labeled C2A domain of synaptotagmin I as a target-specific molecular probe for noninvasive imaging of acute myocardial infarction. J Nucl Med 47:1367–1374
98. Alam IS, Neves AA, Witney TH, Boren J, Brindle KM (2010) Comparison of the C2A domain of synaptotagmin-I and annexin-V as probes for detecting cell death. Bioconjug Chem 21:884–891

99. Tavaré R, De Rosales TM, Blower PJ, Mullen GE (2009) Efficient site-specific radiolabeling of a modified C2A domain of synaptotagmin I with [99mTc(CO)3]+: a new radiopharmaceutical for imaging cell death. Bioconjug Chem 20:2071–2081
100. Hueting R, Tavaré R, Dilworth JR, Mullen GE (2013) Copper-64 radiolabelling of the C2A domain of synaptotagmin I using a functionalised bis(thiosemicarbazone): a pre- and post-labelling comparison. J Inorg Biochem 128:108–111
101. Wang F, Fang W, Zhang MR, Zhao M, Liu B, Wang Z, Hua Z, Yang M, Kumata K, Hatori A, Yamasaki T, Yanamoto K, Suzuki K (2011) Evaluation of chemotherapy response in VX2 rabbit lung cancer with 18F-labeled C2A domain of synaptotagmin I. J Nucl Med 52:592–599
102. Neves AA, Xie B, Fawcett S, Alam IS, Witney TH, de Backer MM, Summers J, Hughes W, McGuire S, Soloviev D, Miller J, Howat WJ, Hu DE, Rodrigues TB, Lewis DY, Brindle KM (2017) Rapid imaging of tumor cell death in vivo using the C2A domain of synaptotagmin-I. J Nucl Med 58:881–887
103. Reubi JC, Maecke HR (2008) Peptide-based probes for cancer imaging. J Nucl Med 49:1735–1738
104. Burtea C, Laurent S, Lancelot E, Ballet S, Murariu O, Rousseaux O, Port M, Elst LV, Corot C, Mueller RN (2009) Peptidic targeting of phosphatidylserine for the MRI detection of apoptosis in atherosclerotic plaques. Mol Pharm 6:1903–1919
105. Desai TJ, Toombs JE, Minna JD, Brekken RA, Udugamasooriya DG (2016) Identification of lipid-phosphatidylserine (PS) as the target of unbiasedly selected cancer specific peptide-peptoid hybrid PPS1. Oncotarget 7:30678–30690
106. Shao R, Xiong C, Wen X, Gelovani JG, Li C (2007) Targeting phosphatidylserine on apoptotic cells with phages and peptides selected from a bacteriophage display library. Mol Imaging 6:417–426
107. Richter S, Wuest F (2014) 18F-Labeled peptides: the future is bright. Molecules 19:20536–20556
108. Kapty J, Kniess T, Wuest F, Mercer JR (2011) Radiolabeling of phosphatidylserine-binding peptides with prosthetic groups N-[6-(4-[18F] fluorobenzylidene)-aminooxyhexyl]maleimide ([18F]FBAM) and N-succinimidyl-4-[18F]fluorobenzoate ([18F] SFB). Appl Radiat Isot 69:1218–1225
109. Wuest M, Perreault A, Kapty J, Richter S, Foerster C, Bergman C, Way J, Mercer J, Wuest F (2015) Radiopharmacological evaluation of (18)F-labeled phosphatidylserine-binding peptides for molecular imaging of apoptosis. Nucl Med Biol 42:864–874
110. Kapty J, Banman S, Goping IS, Mercer JR (2012) Evaluation of phosphatidylserine-binding peptides targeting apoptotic cells. J Biomol Screen 17:1293–1301
111. Khoshbakht S, Beiki D, Geramifar B, Kobarfard F, Sabzevari O, Amini M, Shahhosseini S (2016) 18FDG-labeled LIKKPF: a PET tracer for apoptosis imaging. J Radioanal Nucl Chem 310:413–421
112. Ben Azzouna R, Guez A, Benali K, Al-Shoukr F, Gonzalez W, Karoyan P, Rouzet F, Le Guludec D (2017) Synthesis, gallium labelling and characterization of P04087, a functionalized phosphatidylserine-binding peptide. EJNMMI Radiopharm Chem 2:3
113. Xiong C, Brewer K, Song S, Zhang R, Lu W, Wen X, Li C (2011) Peptide-based imaging agents targeting phosphatidylserine for the detection of apoptosis. J Med Chem 54:1825–1835
114. Igarashi K, Kaneda M, Yamaji A, Saido TC, Kikkawa U, Ono Y, Inoue K, Umeda M (1995) A novel phosphatidylserine-binding peptide motif defined by an anti-idiotypic monoclonal antibody. Localization of phosphatidylserine-specific binding sites on protein kinase C and phosphatidylserine decarboxylase. J Biol Chem 270:29075–29078
115. Song S, Xiong C, Lu W, Ku G, Huang G, Li C (2013) Apoptosis imaging probe predicts early chemotherapy response in preclinical models: a comparative study with 18F-FDG PET. J Nucl Med 54:104–110
116. Perreault A, Richter S, Bergman C, Wuest M, Wuest F (2016) Targeting phosphatidylserine with a 64Cu-labeled peptide for molecular imaging of apoptosis. Mol Pharm 13:3564–3577
117. Nock BA, Maina T, Krenning EP, de Jong M (2014) To serve and protect': enzyme inhibitors as radiopeptide escorts promote tumor targeting. J Nucl Med 55:121–127
118. Langer M, Beck-Sickinger AG (2001) Peptides as carrier for tumor diagnosis and treatment. Curr Med Chem Anticancer Agents 1:71–93
119. Thapa N, Kim S, So IS, Lee BH, Kwon IC, Choi K, Kim IS (2008) Discovery of a phosphatidylserine-recognizing peptide and its utility in molecular imaging of tumour apoptosis. J Cell Mol Med 12:1649–1660
120. Kim S, Bae SM, Seo J, Cha K, Piao M, Kim SJ, Son HN, Park RW, Lee BH, Kim IS (2015) Advantages of the phosphatidylserine-recognizing peptide PSP1 for molecular imaging of tumor apoptosis compared with annexin V. PLoS ONE 10:e0121171
121. Shukla SP, Udugamasooriya DG (2017) A mini-library system to investigate non-essential residues of lipid-phosphatidylserine (PS) binding peptide-peptoid hybrid PPS1. Medchemcomm 8:2208–2215
122. Singh J, Shukla SP, Desai TJ, Udugamasooriya DG (2016) Identification of the minimum pharmacophore of lipid-phosphatidylserine (PS) binding peptide-peptoid hybrid PPS1D1. Bioorg Med Chem 24:4470–4477
123. Shukla SP, Manarang JC, Udugamasooriya DG (2017) A unique mid-sequence linker used to multimerize the lipid-phosphatidylserine (PS) binding peptide-peptoid hybrid PPS1. Eur J Med Chem 137:1–10
124. Zheng H, Wang F, Wang Q, Gao J (2011) Cofactor-free detection of phosphatidylserine with cyclic peptides mimicking lactadherin. J Am Chem Soc 133:15280–15283
125. Hosseini AS, Zheng H, Gao J (2014) Understanding lipid recognition by protein-mimicking cyclic peptides. Tetrahedron 70:7632–7638
126. Stafford JH, Hao G, Best AM, Sun X, Thorpe PE (2013) Highly specific PET imaging of prostate tumors in mice with an iodine-124-labeled antibody fragment that targets phosphatidylserine. PLoS ONE 8:e84864
127. Zhang L, Zhou H, Belzile O, Thorpe P, Zhao D (2014) Phosphatidylserine-targeted bimodal liposomal nanoparticles for in vivo imaging of breast cancer in mice. J Control Release 183:114–123
128. Koulov AV, Stucker KA, Lakshmi C, Robinson JP, Smith BD (2003) Detection of apoptotic cells using a synthetic fluorescent sensor for membrane surfaces that contain phosphatidylserine. Cell Death Differ 10:1357–1359
129. Ngo HT, Liu X, Jolliffe KA (2012) Anion recognition and sensing with Zn(II)-dipicolylamine complexes. Chem Soc Rev 41:4928–4965
130. Plaunt AJ, Harmatys KM, Wolter WR, Suckow MA, Smith BD (2014) Library synthesis, screening, and discovery of modified Zinc(II)-Bis(dipicolylamine) probe for enhanced molecular imaging of cell death. Bioconjug Chem 25:724–737
131. Oltmanns D, Zitzmann-Kolbe S, Mueller A, Bauder-Wuest U, Schaefer M, Eder M, Haberkorn U, Eisenhut M. Zn (2011) (II)-bis(cyclen) complexes and the imaging of apoptosis/necrosis. Bioconjug Chem 22:2611–2624
132. Wang H, Wu Z, Li S, Hu K, Tang G (2017) Synthesis and evaluation of a radiolabeled bis-zinc(II)-cyclen complex as a potential probe for in vivo imaging of cell death. Apoptosis 22:585–595
133. Wyffels L, Gray BD, Barber C, Moore SK, Woolfenden JM, Pak KY, Liu Z (2011) Synthesis and preliminary evaluation of

radiolabeled bis(zinc(II)-dipicolylamine) coordination complexes as cell death imaging agents. Bioorg Med Chem 19:3425–3433
134. Sun T, Tang G, Tian H, Hu K, Yao S, Su Y, Wang C (2015) Positron emission tomography imaging of cardiomyocyte apoptosis with a novel molecule probe [18F]FP-DPAZn2. Oncotarget 6:30579–30591
135. Wang H, Tang X, Tang G, Huang T, Liang X, Hu K, Deng H, Yi C, Shi X, Wu K (2013) Noninvasive positron emission tomography imaging of cell death using a novel small-molecule probe, (18)F labeled bis(zinc(II)-dipicolylamine) complex. Apoptosis 18:1017–10927
136. Wen F, Nie D, Hu K, Tang G, Yao S, Tang C (2017) Semi-automatic synthesis and biodistribution of N-(2-(18) F-fluoropropionyl)-bis(zinc (II)-dipicolylamine) ((18)F-FP-DPAZn2) for AD model imaging. BMC Med Imaging 17:27
137. Wang X, Feng H, Zhao S, Xu J, Wu X, Cui J, Zhang Y, Qin Y, Liu Z, Gao T, Gao Y, Zeng W (2017) SPECT and PET radiopharmaceuticals for molecular imaging of apoptosis: from bench to clinic. Oncotarget 8:20476–20495